Chapter 18

Structures and Properties of Solids

Defects in solids

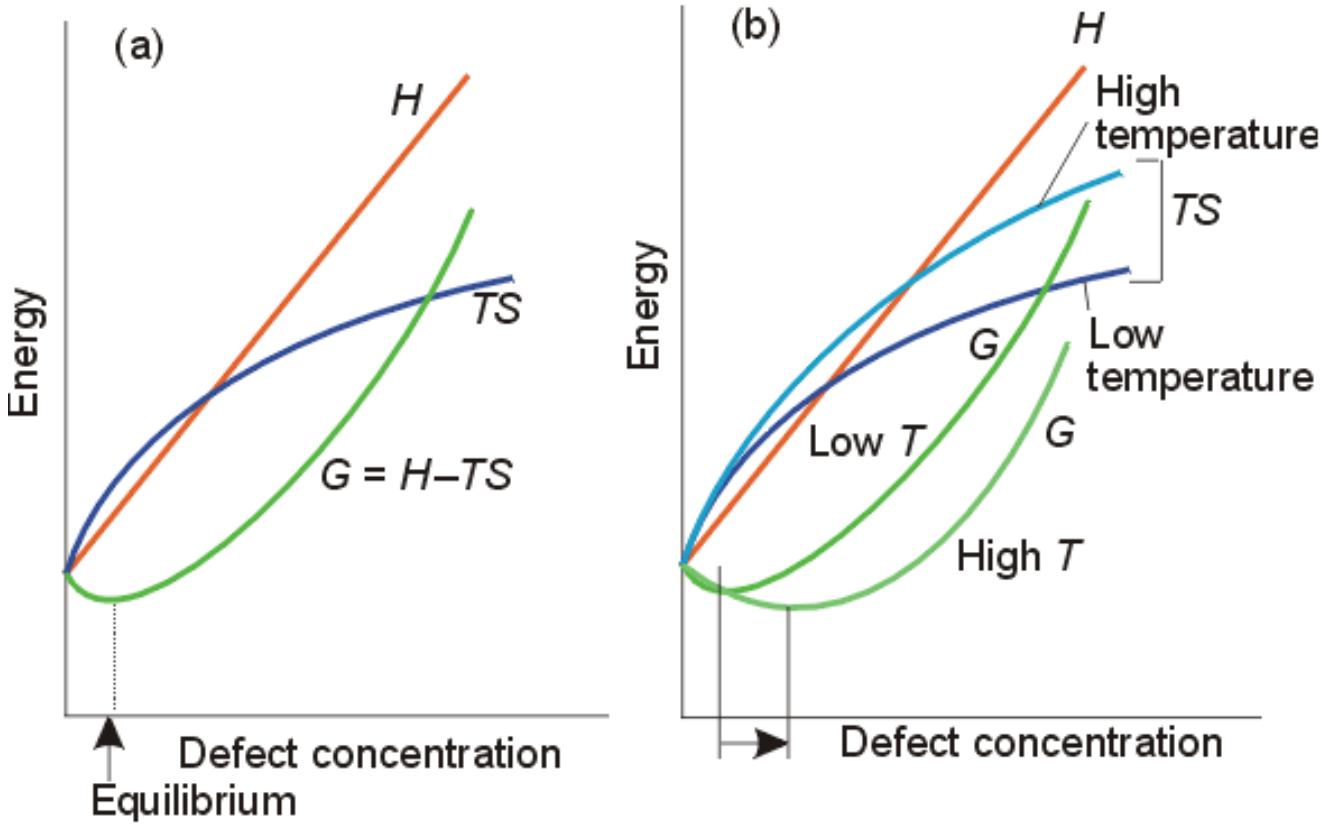

$$G = H - TS$$

18.1

Structural Defects

Intrinsic defects- occur in the pure substance

Extrinsic defects- stem from the presence of impurity

Point defects

Extended defects- in one, two or three dimension

Intrinsic Point Defects

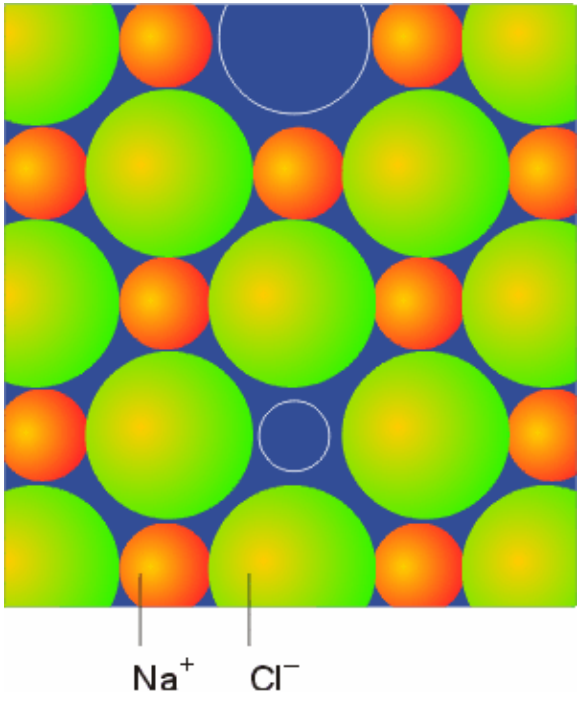

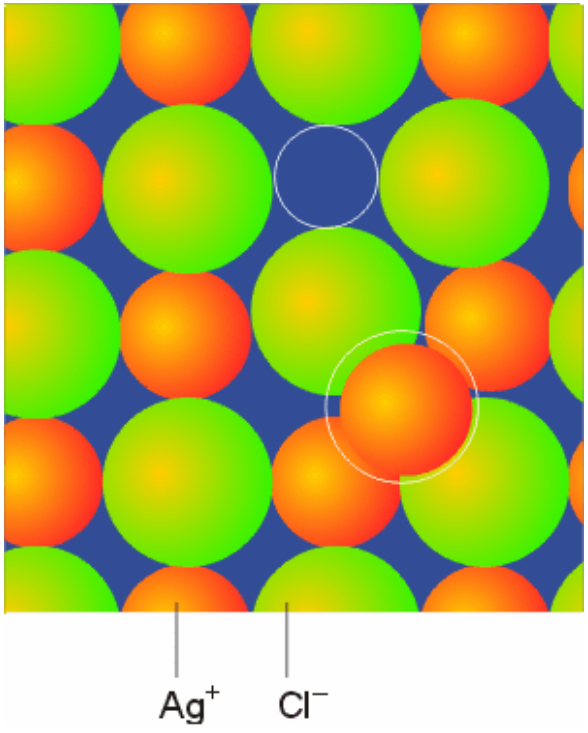

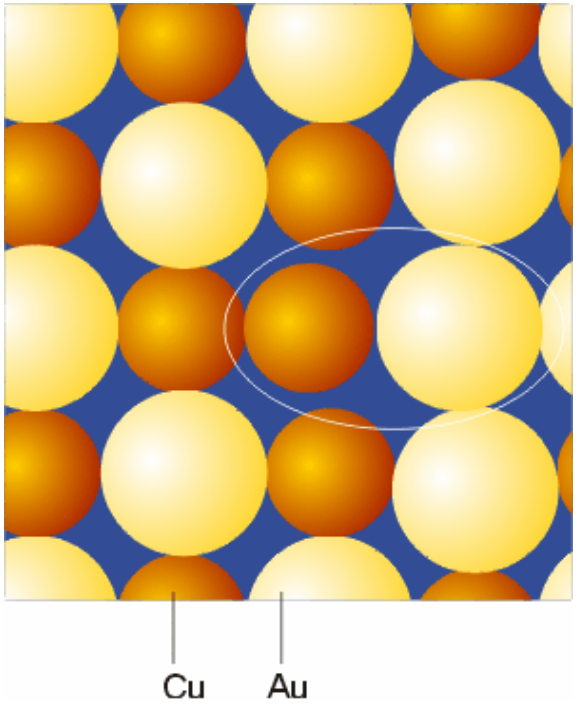

Shottky defect-

Missing ion-pair

Frenkel defect-

misplacing ions to interstitial

Atom exchange defect

Extrinsic Point Defects

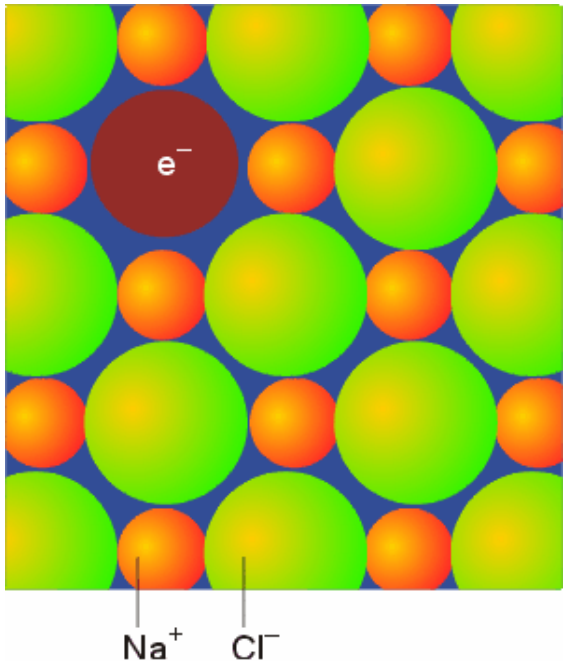

“F-center” defect

“*Farbenzenter*” German word for color center

Defect sites of FeO

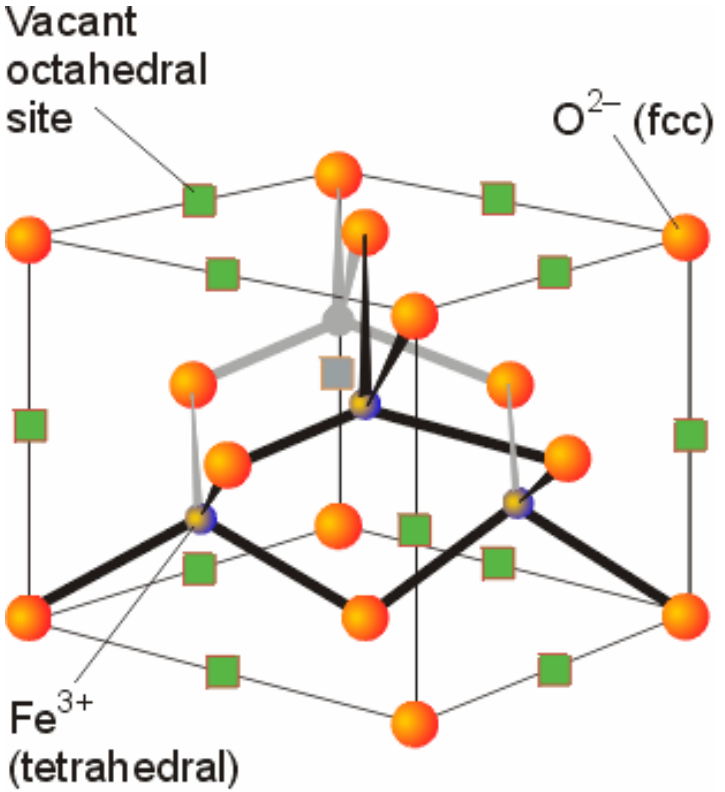

Fe^{2+}
O_h sites

Nonstoichiometry of FeOx

One Fe(II) vacancy is charge-compensated by

2 Fe(II) $\rightarrow$2 Fe(III)

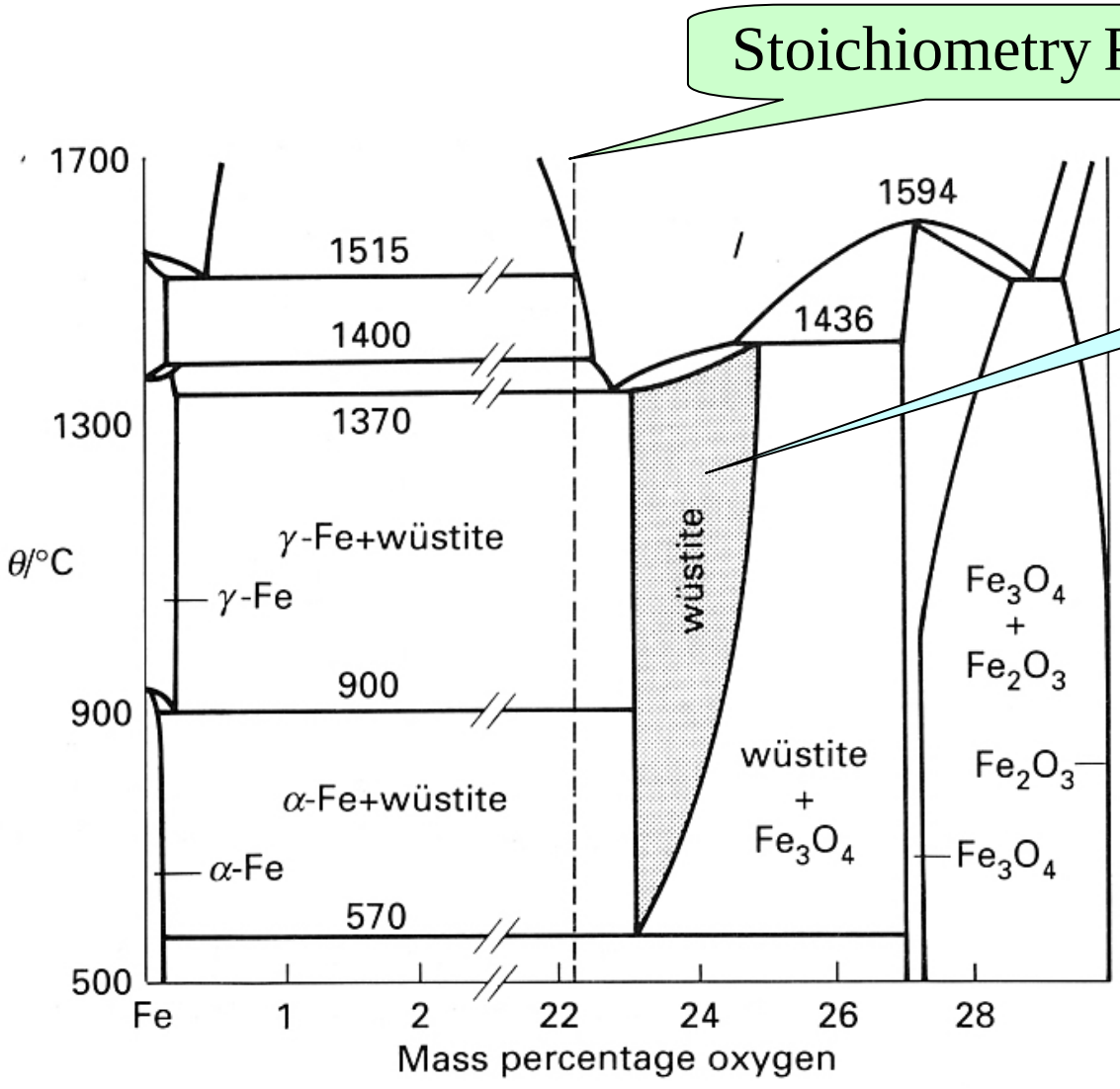

Jeff Weissman/ photographic Guide to Mineral

Phase diagram of Iron Oxides as a Function of Oxygen Content

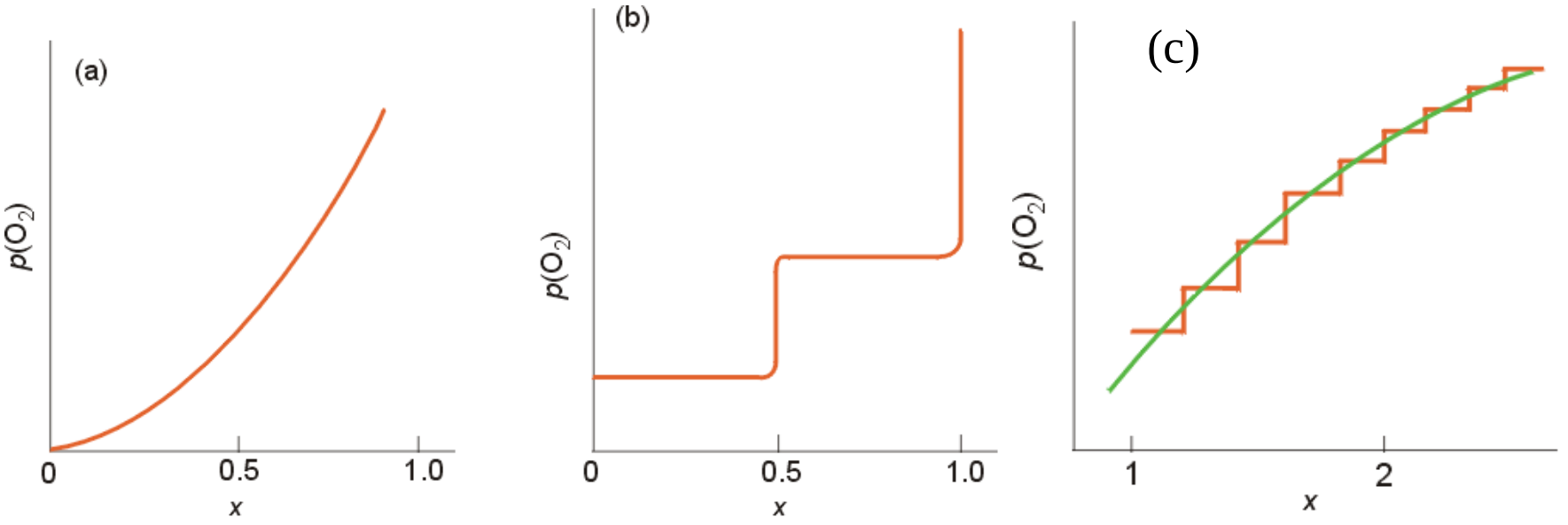

Variation of partial pressure of oxygen with composition at constant pressure for (a) a nonstoichiometric oxide; (b) a stoichiometric pair of metal oxides MO and MO_2; (c) a series of closely spaced discrete phases. The axis *x* is the atom ratio in MO_x.

Plane Defects

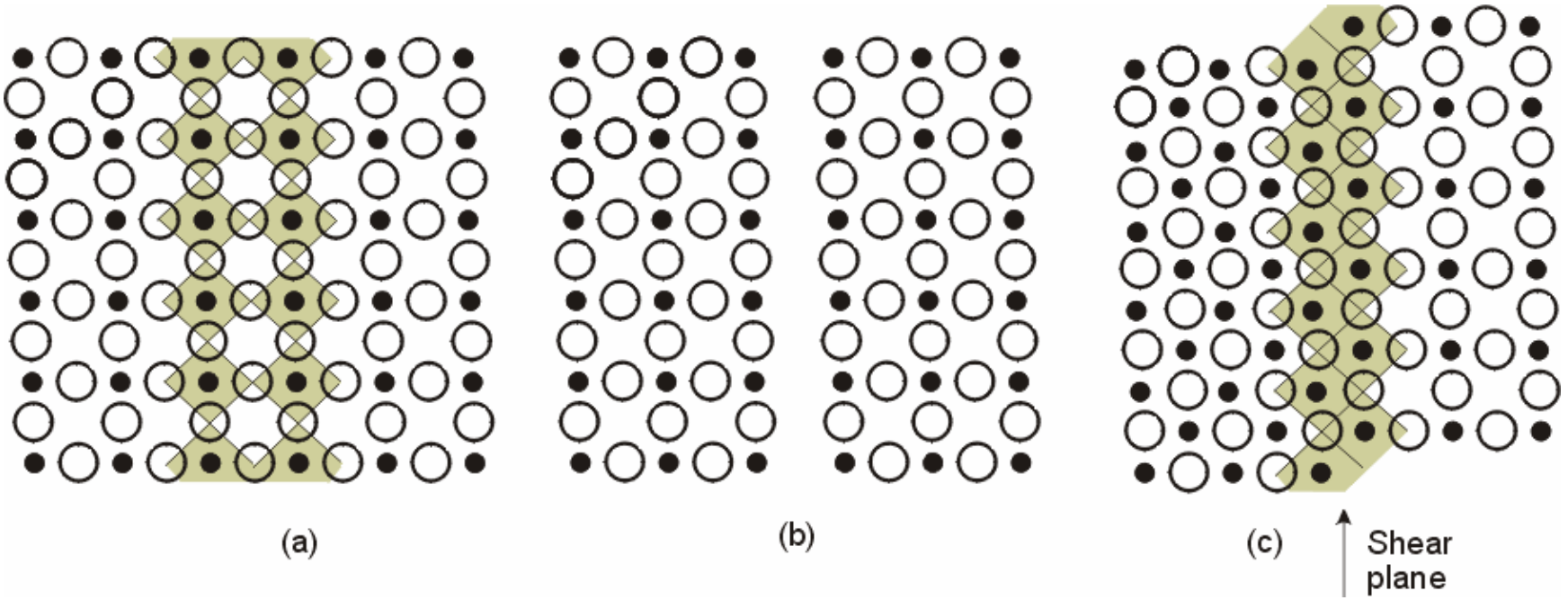

Shear plane: formation upon "Oxygen- removal"

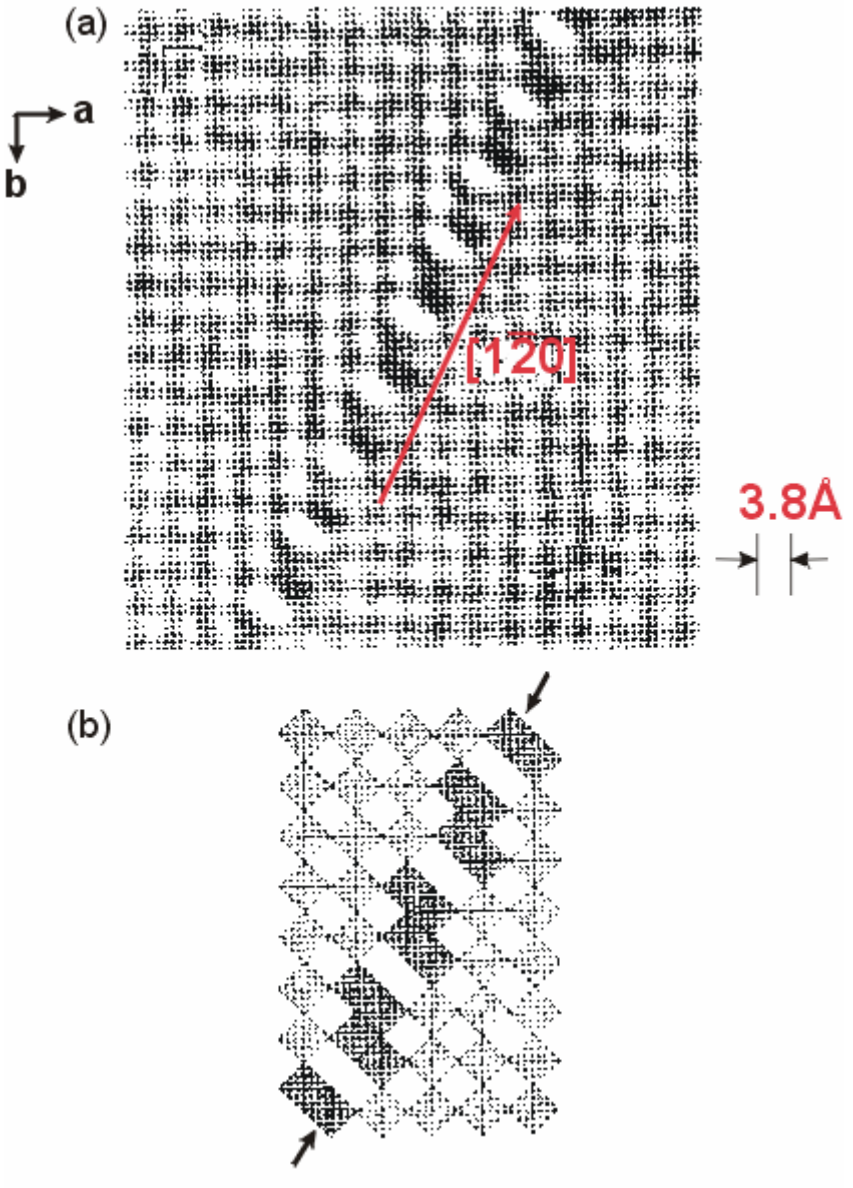

Shear plane

High resolution SEM on ($1\bar{2}0$) in WO_{3-x}

Insertion of oxygen

Group V, VI, and VII transition metal oxides are good catalysts for selective oxidation of hydrocarbons.

e.g. V_2O_5, MoO_3, WO_3
V VI VI

Reasons for high activity and selectivity in the insertion of oxygen

Formation of a oxygen vacancy or a shear plane?

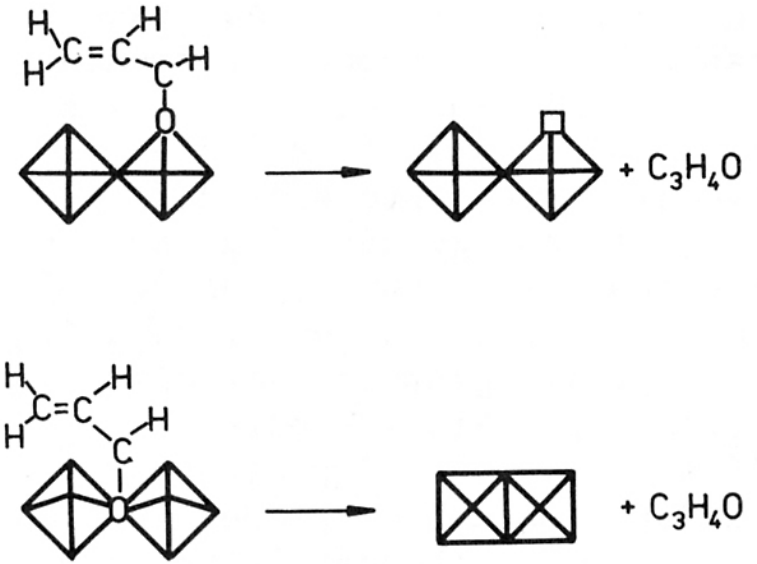

Figure 9. Mechanism of the insertion of oxygen into hydrocarbon molecule on oxide catalysts with point defects (a) and shear structures (b).

Surface structure

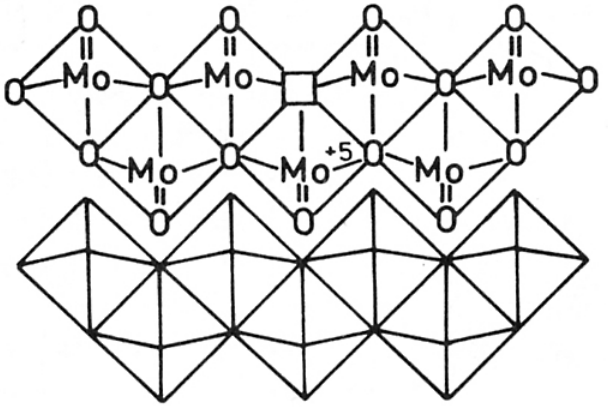

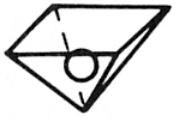

$g_x = 1{,}943$
$g_y = 1{,}960$
$g_z = 1{,}868$

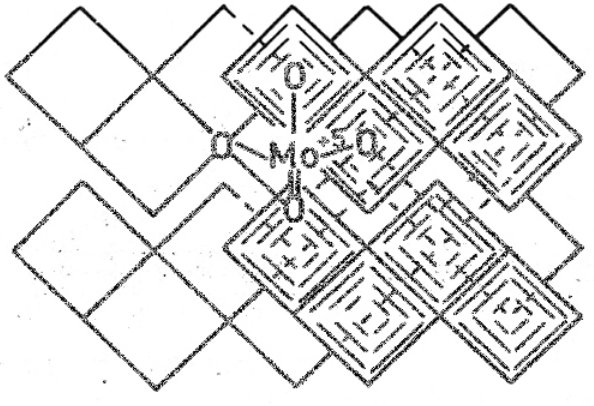

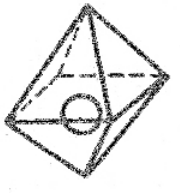

$g_x = 1{,}943$
$g_y = 1{,}954$
$g_z = 1{,}879$

Observed in experiments

Figure 7. Generation of oxygen vacancies and shear planes in MoO_3 structure.

Ion Conductivity

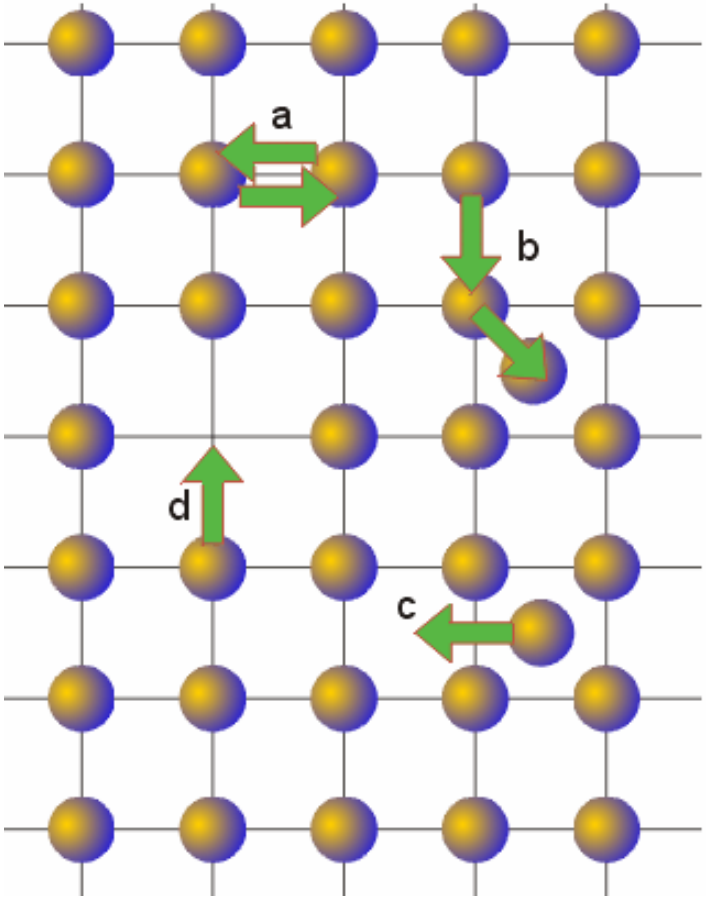

Diffuse mechanisms for ions or atoms in a solid:

(a) exchange

(b) interstitialcy

(c) interstitial

(d) vacancy

Diffusion

$$\frac{\partial c}{\partial t} = D\frac{\partial^2 c}{\partial x^2}$$

D: Diffusion coefficient

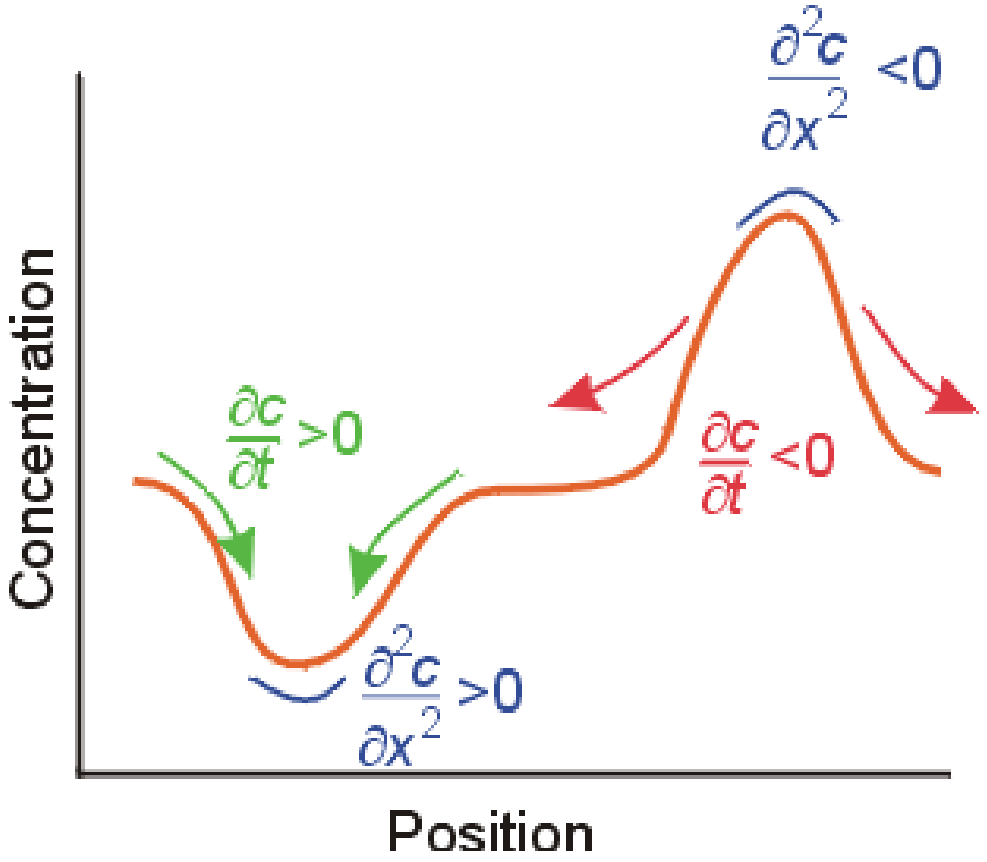

Activation Energy of Ion-Conductor

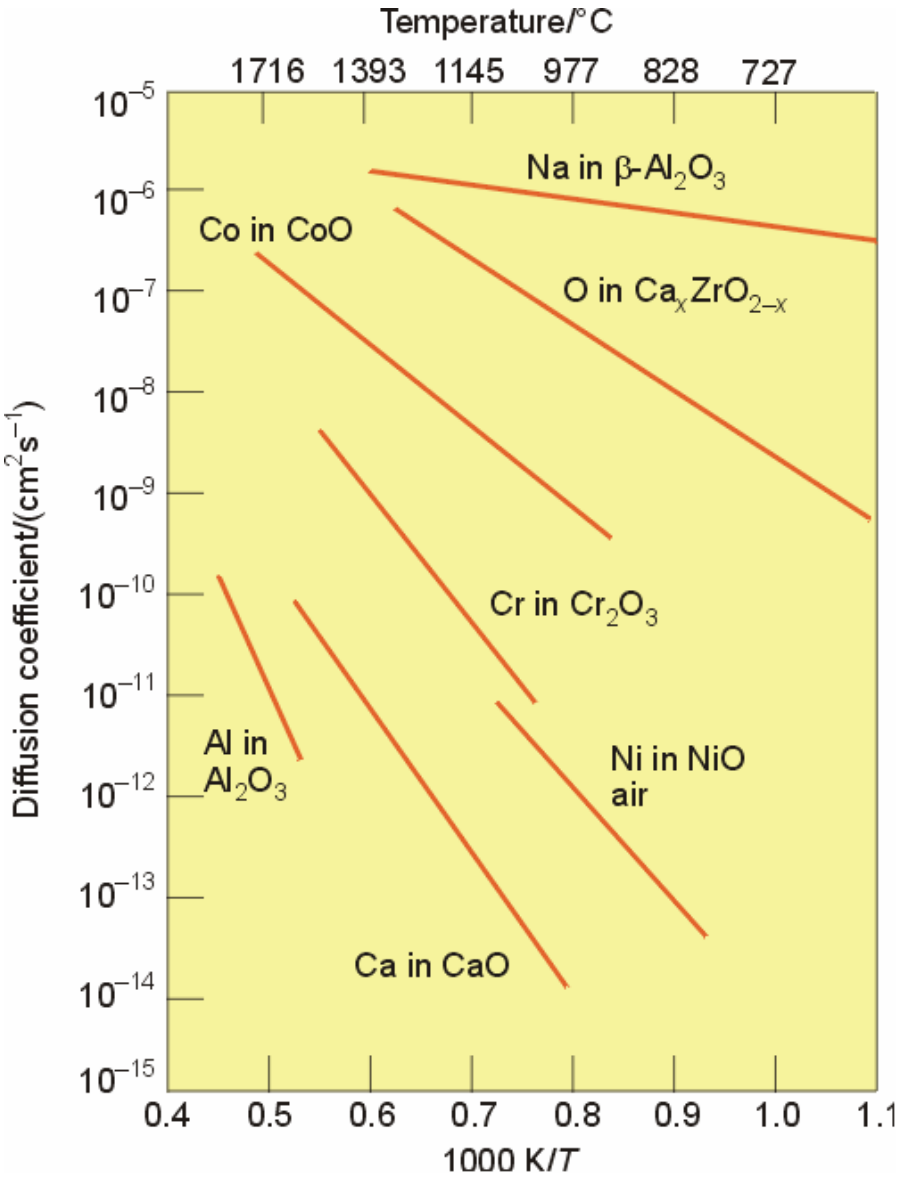

Arrhenius plot of the logarithm of the diffusion coefficient of the mobile ion

$$D = D_0 \exp(-Ea/RT)$$

Ag_2HgI_4

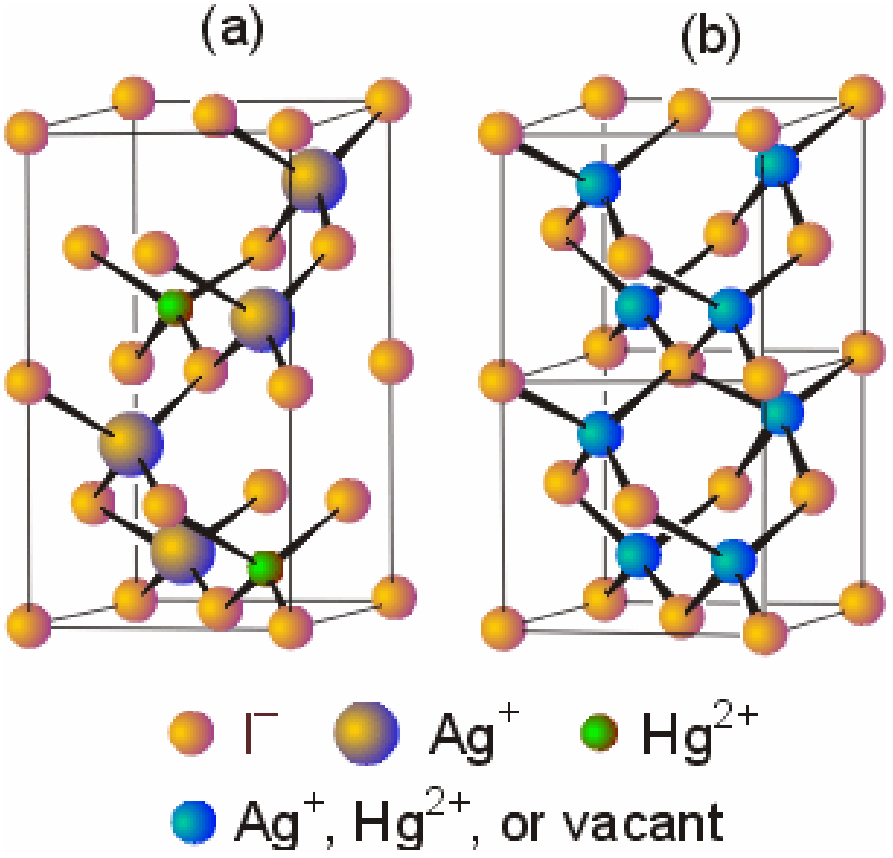

(a) low-temperature order structure

(b) high-temperature disordered structure

a Ag^+-conductor

b-Alumina a Na^+-conductor

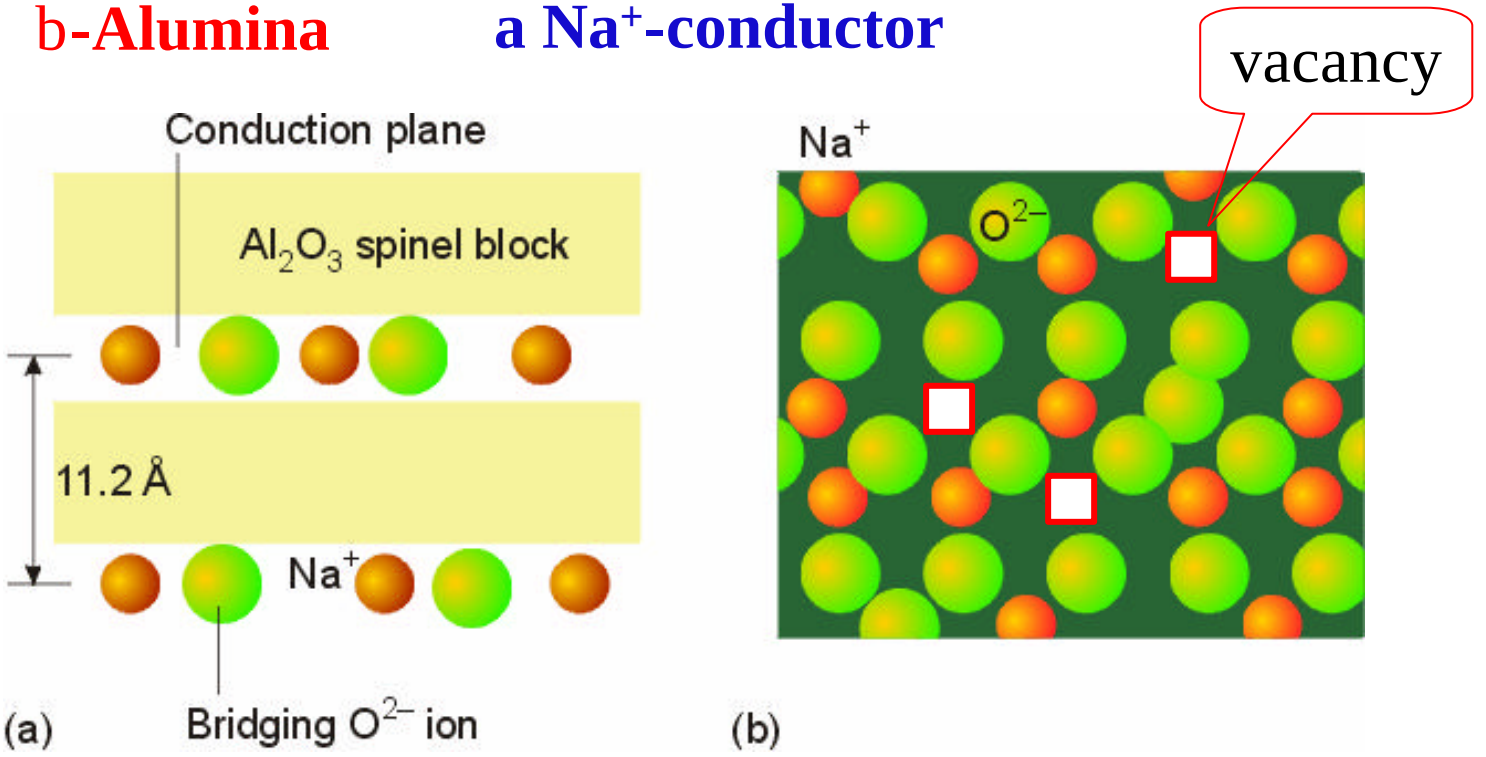

Side view Conducting plane

an O^{2-}-conductor

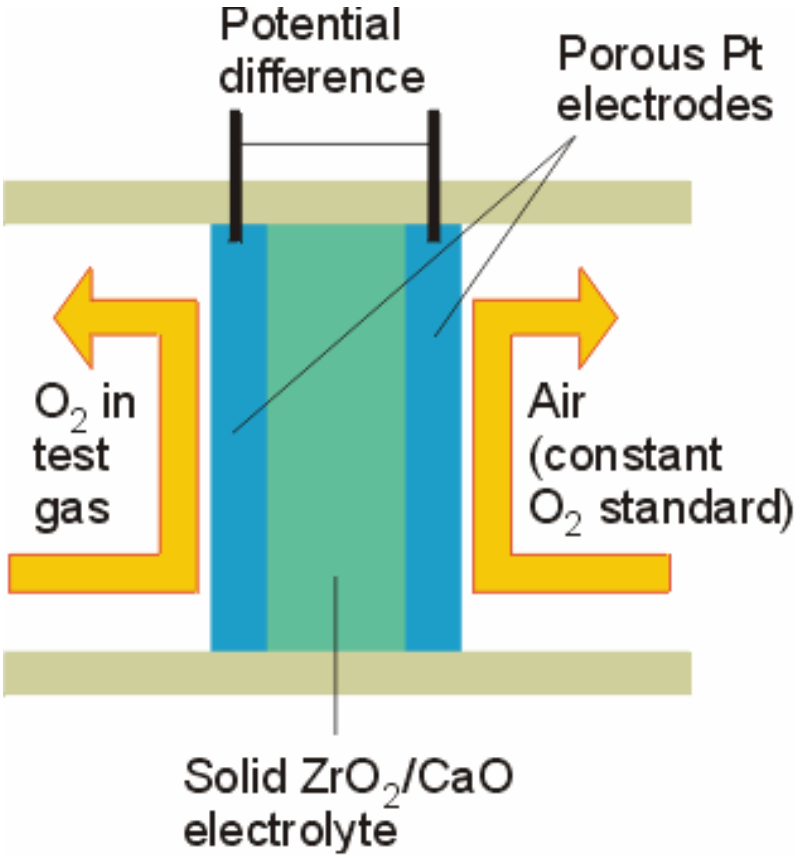

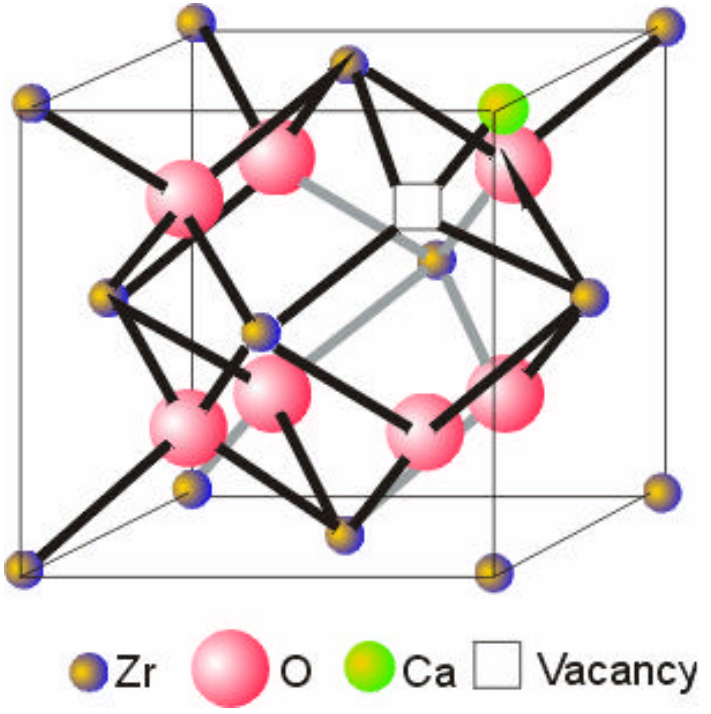

Solid Oxide Fuel Cell (SOFC)

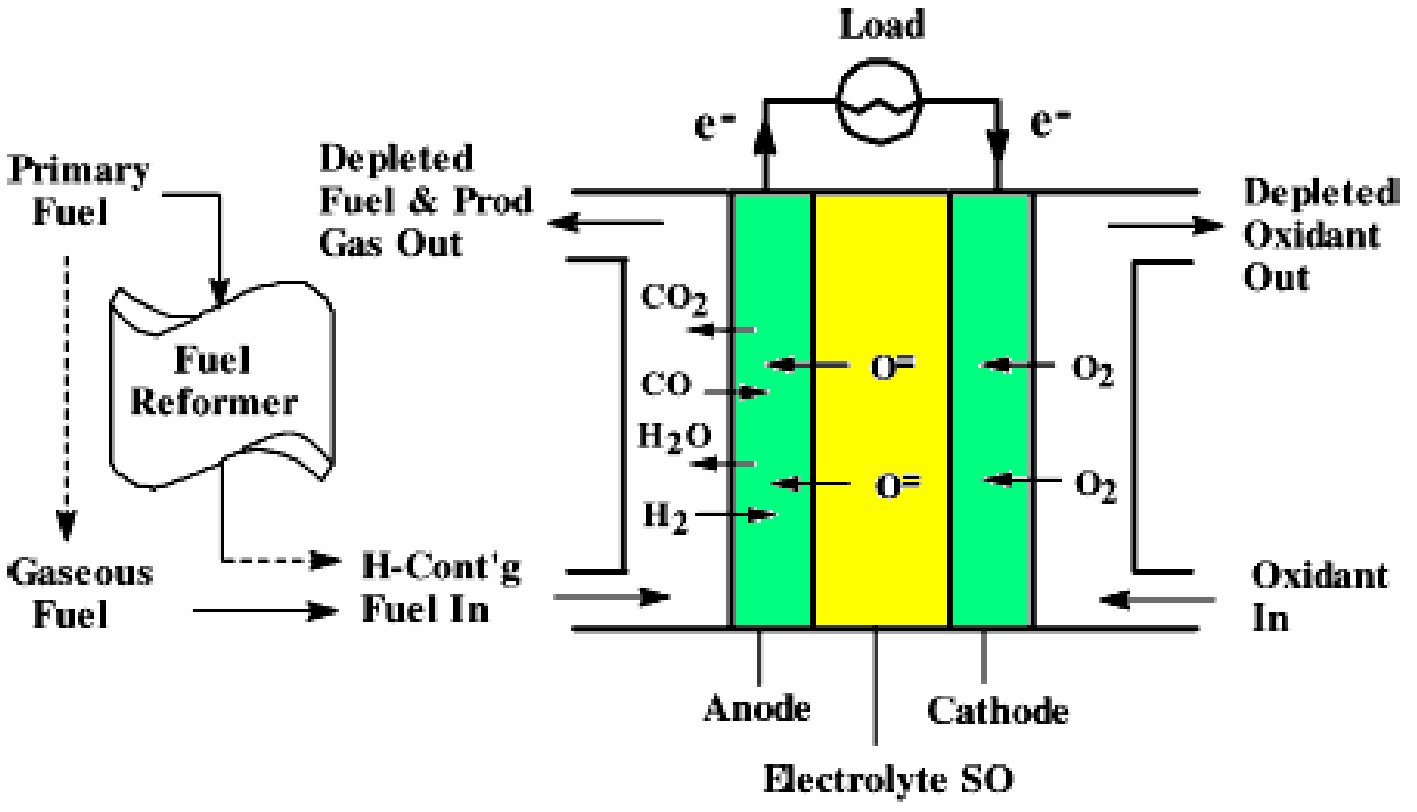

Anode (Fuel) Reaction: $H_2 + O^= \rightarrow H_2O + 2\,e^-$

$CO + O^= \rightarrow CO_2 + 2\,e^-$

Cathode (Oxidant) Reaction: $O_2 + 2\,e^- \rightarrow 2\,O^=$

Total Reaction: $H_2 + CO + O_2 \rightarrow H_2O + CO_2$

Table 18.2 Monoxides of the Period 4 metals

Compound	Structure	Stoichiometry MO_x	Electrical properties
CaO_x	Rock salt	1	Insulator
TiO_x	Rock salt	0.65–1.25	Metallic
VO_x [a]	Rock salt	0.79–1.29	Metallic
MnO_x	Rock salt	1–1.15	Semiconductor
FeO_x	Rock salt	1.04–1.17	Semiconductor
CoO_x	Rock salt	1–1.01	Semiconductor
NiO_x	Rock salt	1–1.001	Semiconductor
CuO_x	PtS	1	Semiconductor
ZnO_x	Wurtzite	Slight Zn excess	Wide gap n-type semiconductor

[a]At low temperatures, VO adopts a less symmetrical structure.

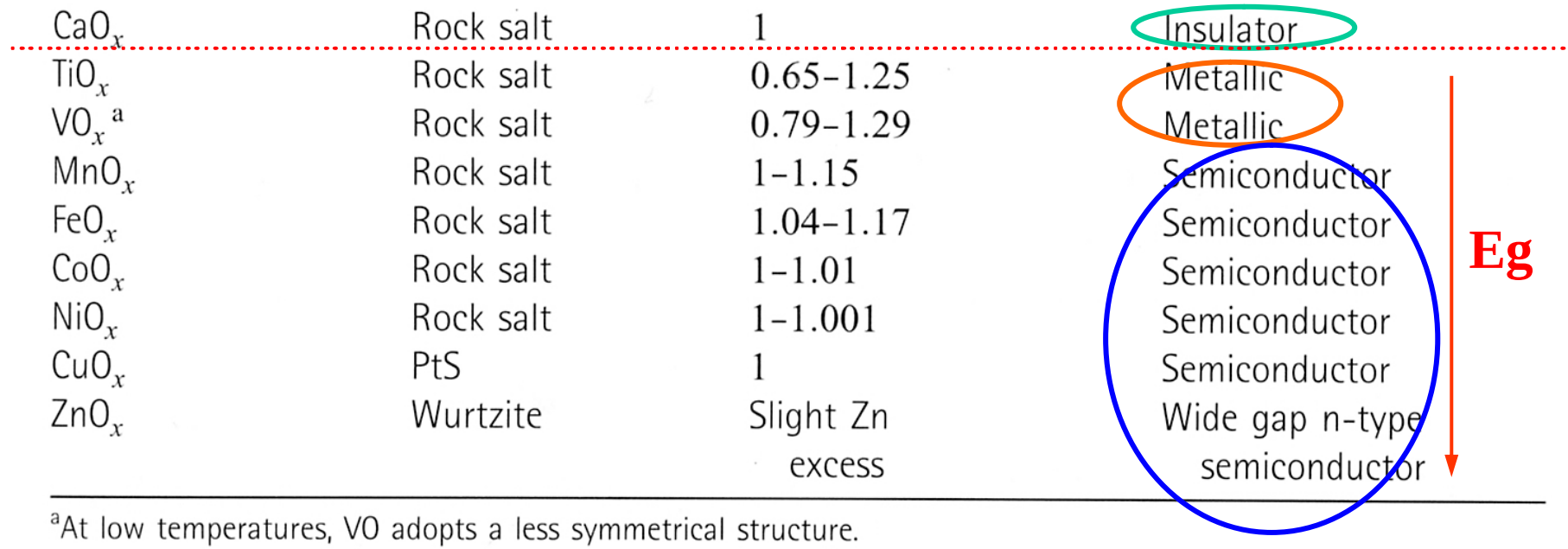

Overlapping of d-Orbitals of Early Transition Metal Elements in the Oxide Structures

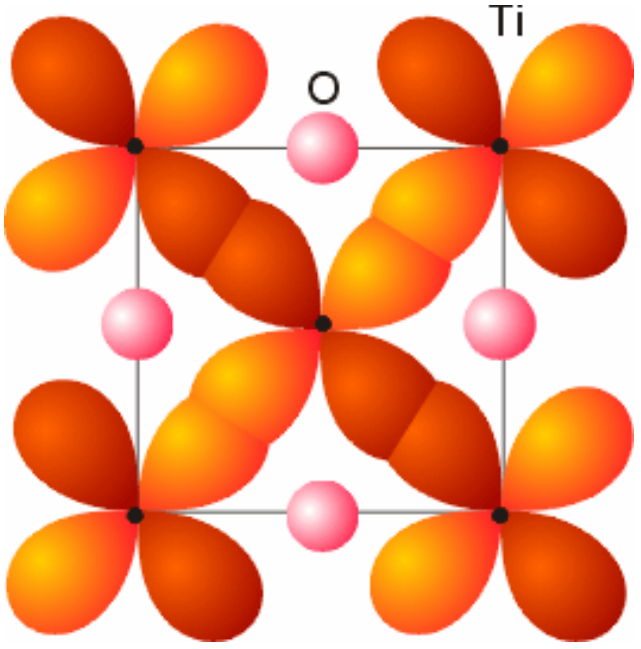

Energy Level Diagram of Early Transition Metal Elements in the Oxide Structures

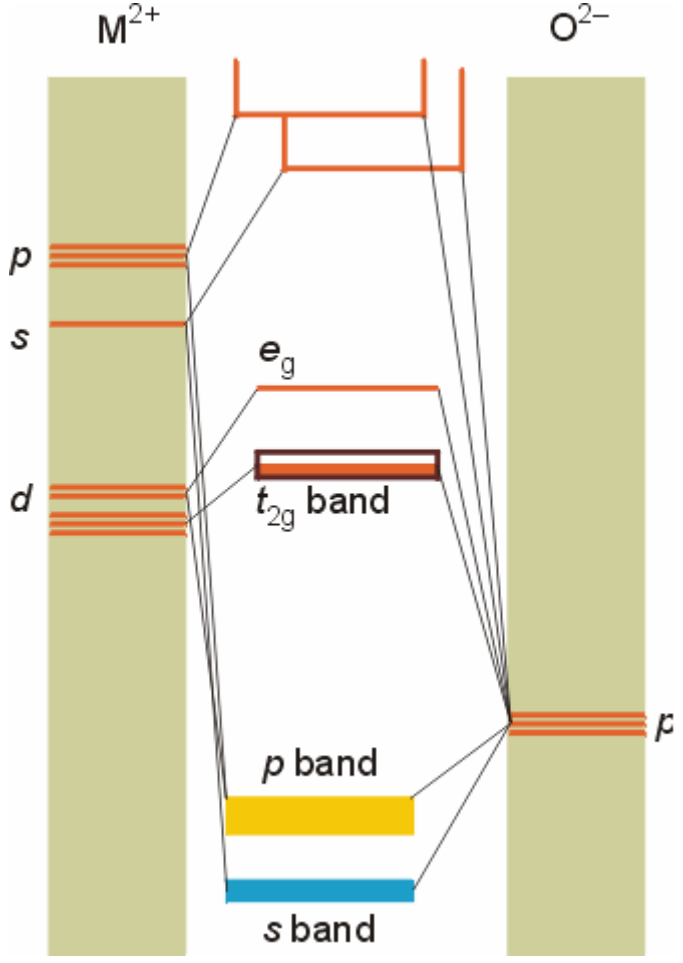

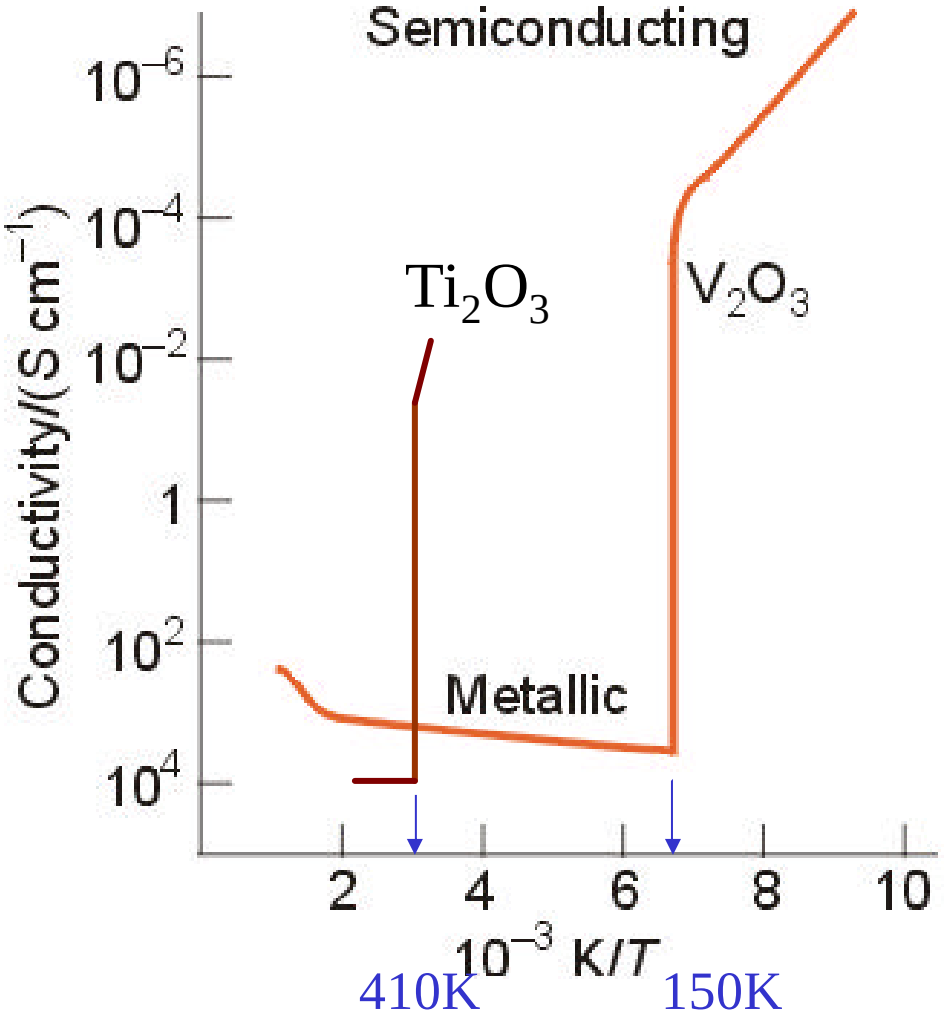

Corundum structure

α-Al_2O_3

O^{2-} : hcp

Al^{3+} : 2/3 O_h sites

Cr(III) doped α-Al_2O_3

$\Rightarrow$ ruby

Cr_2O_3, Fe_2O_3 insulators

& antiferromagnetic

Magnetic Properties of Materials with Long-Range Ordered Spins

Ferromagnetic

Antiferromagnetic

J: energy of interaction of the spins on different ions

If J< kT paramagnetic

Property of individual ion

If J> kT => { **Ferromagnetic** / **Antiferromagnetic**

Cooperative magnetism

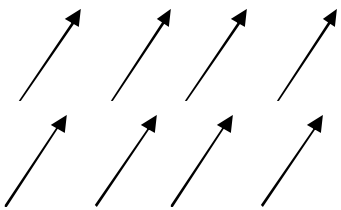

Ferromagnetic

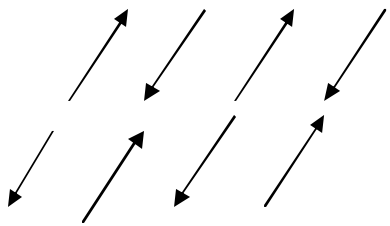

Antiferromagnetic

Molar magnetic susceptibility, χ

In **a magnetic field, H**, **the magnetic induction, B**, in the material is

B = H + 4pI, where **I= magnetic moment/ volume**

magnetic permeability, ***P*** = B/H = 1 + (4 π I)/H = 1 + 4 π κ

magnetic susceptibility, k = I/H

Molar magnetic susceptibility

c = k **F/d,** where F= formula weight

d= density of the material

Curie-Weiss Law: c = **C/(T + q),**

C: Curie constant; q: Weiss constant

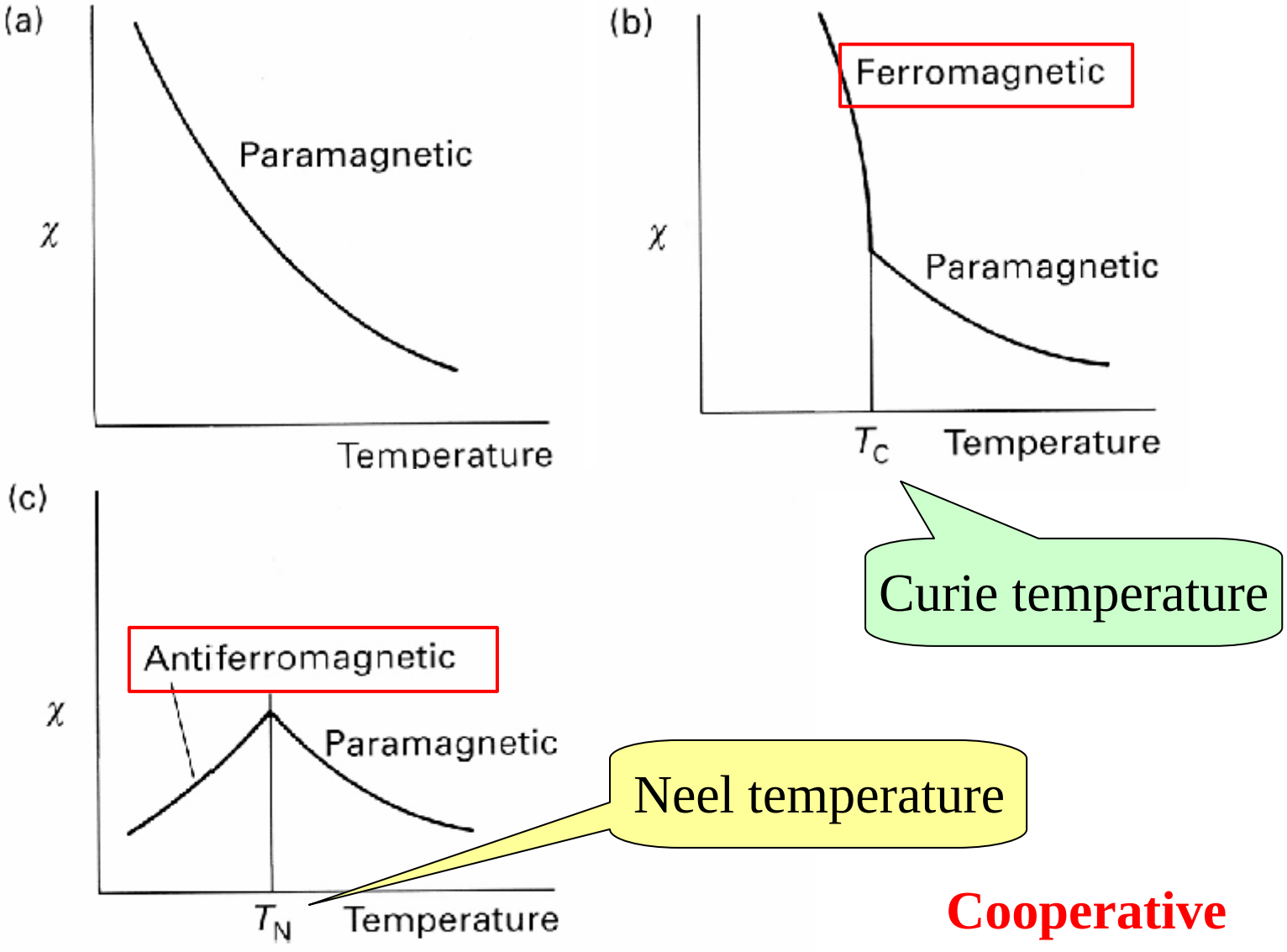

B18.3 Comparison of the temperature dependence of paramagnetic, ferromagnetic, and antiferromagnetic substances.

Cooperative magnetism

B18.3

Intercalation Reactions

$$C_{(graphite)} + n\,K(s) \rightarrow CK_n\ (C^{n-}, n\,K^+)$$

$$C_{(graphite)} + n/2\,Br_2(g) \rightarrow CBr_n\ (C^{n+}, n\,Br^-)$$

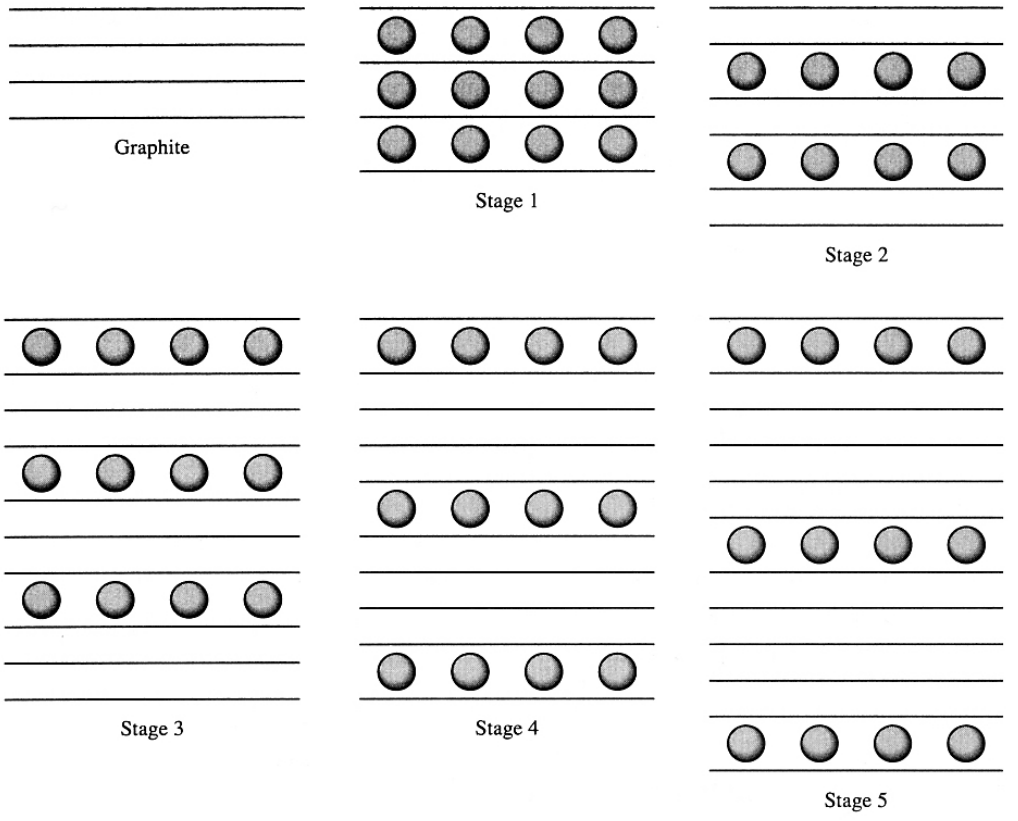

Figure 6.33 Graphite intercalation compounds indicating different staging.

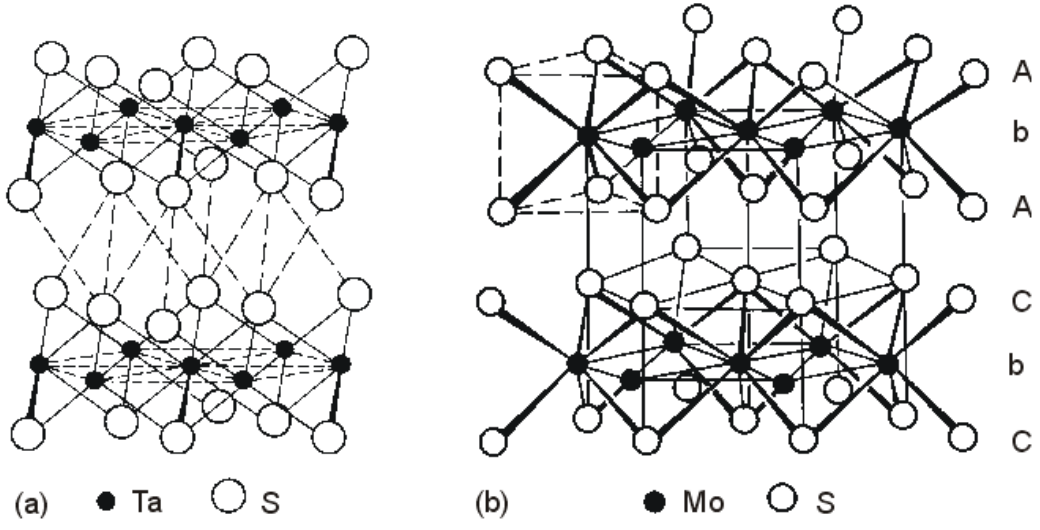

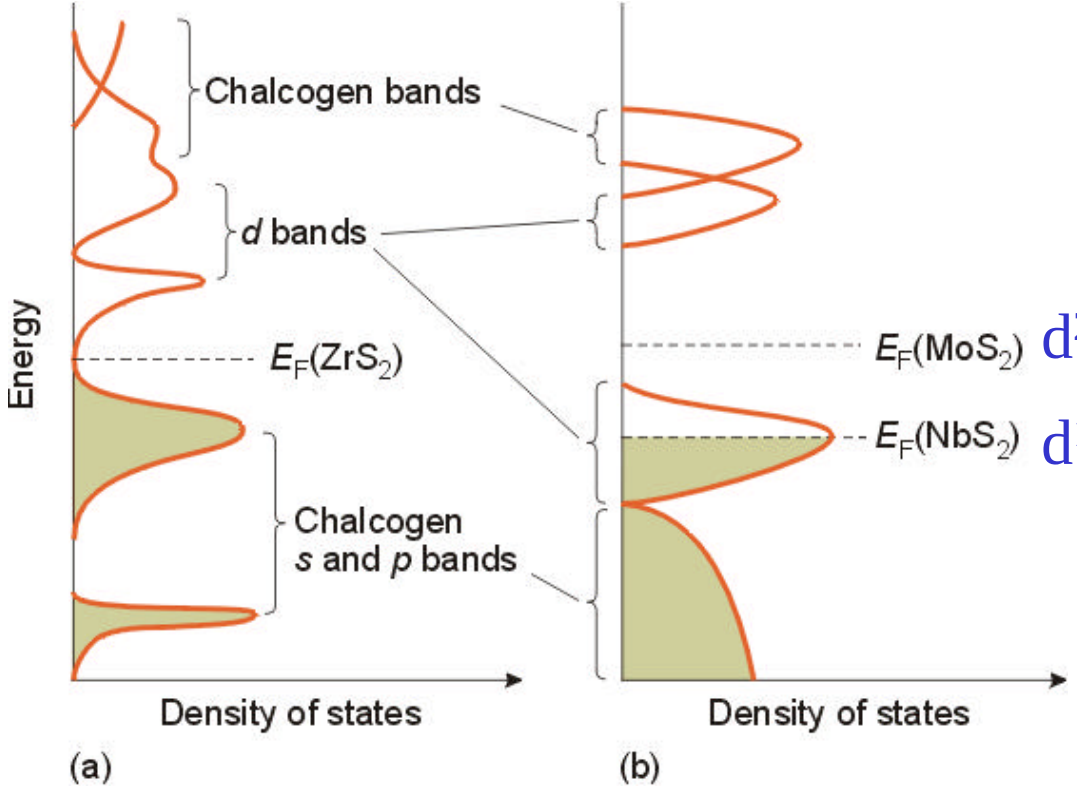

d^2, semiconductor

d^1, metallic

Chemical vapor transport crystal growth

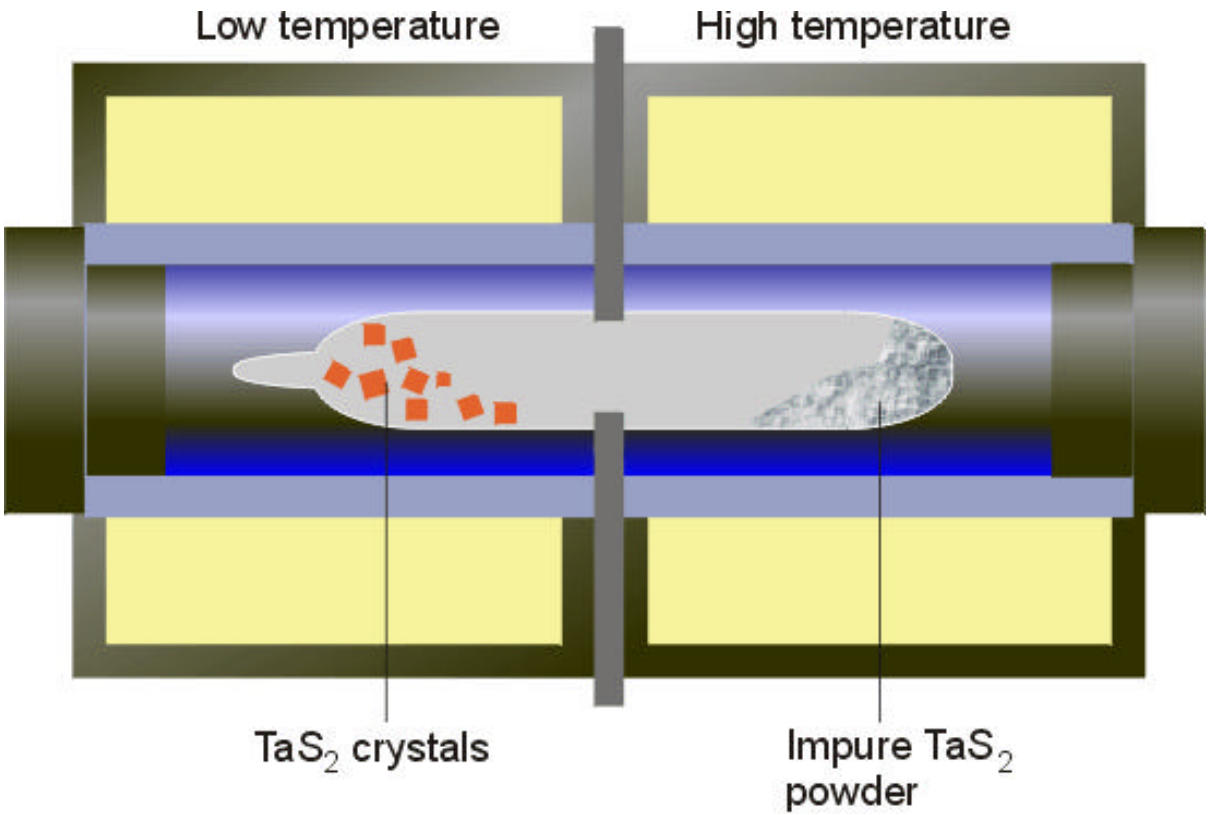

$$TaS_2(s) + 2I_2(g) \underset{750^\circ C}{\overset{850^\circ C}{\rightleftharpoons}} TaI_4(s) + S_2(g)$$

Hosts for Intercalation

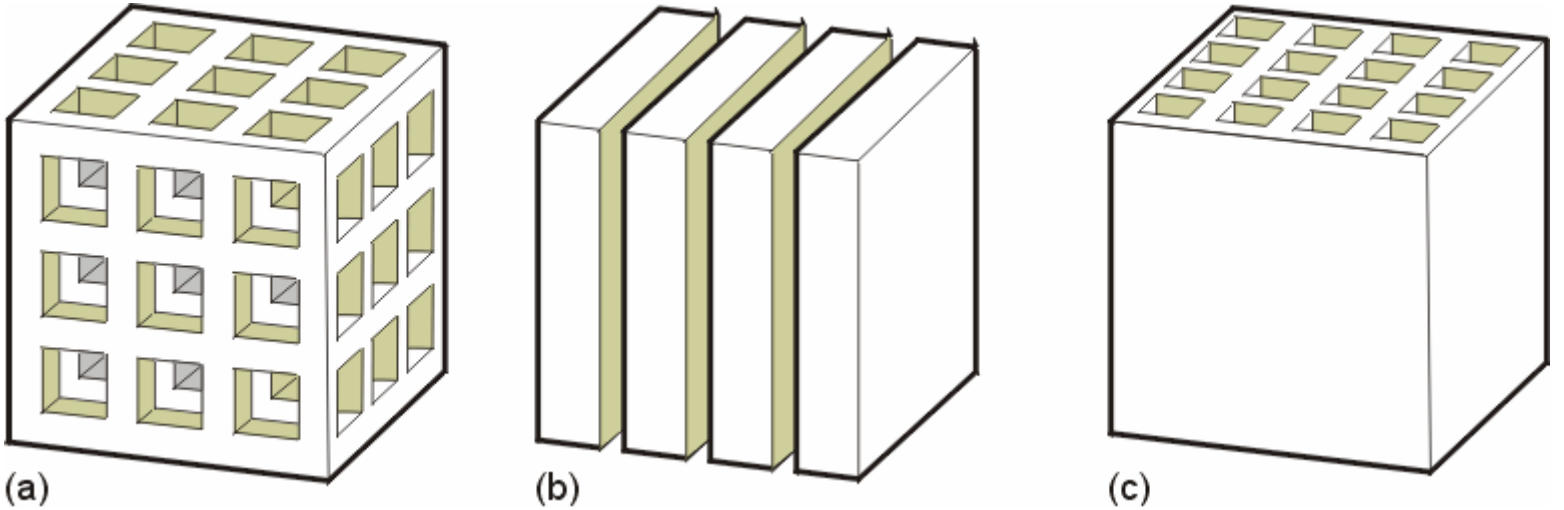

Table 18.6 Some three-dimensional intercalation compounds

Phase	Composition (x)
$Li_x[Mo_6S_8]$	2.4 to 0.6
$Na_x[Mo_6S_8]$	3.6
$Ni_x[Mo_6Se_8]$	1.8
H_xWO_3	0.6
Li_xWO_3	0.6
Li_xNiPS_3	0 to 1.5

Chevrel phases- three-dimensional intercalation

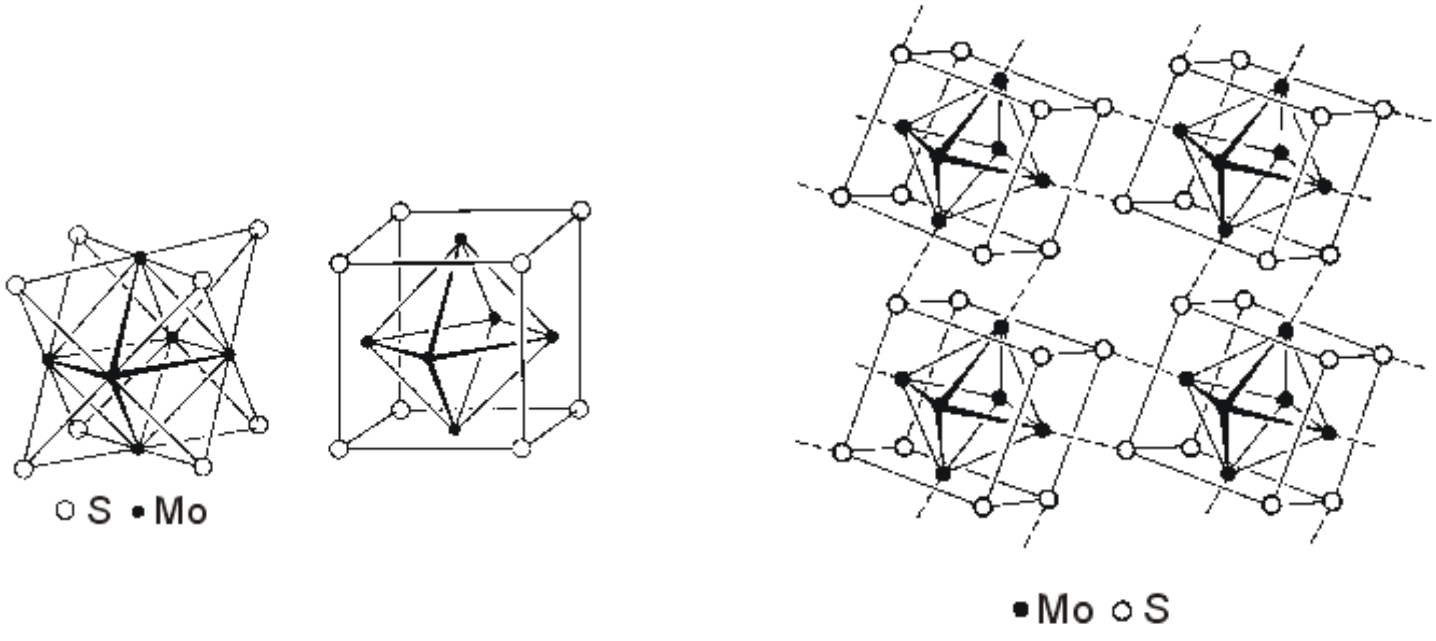

Mo_6S_8 or $M_xMo_6S_8$

M= Li, Mn, Fe, Cd, Pb

$PbMo_6S_8$ superconductor at 14K

18.38-39

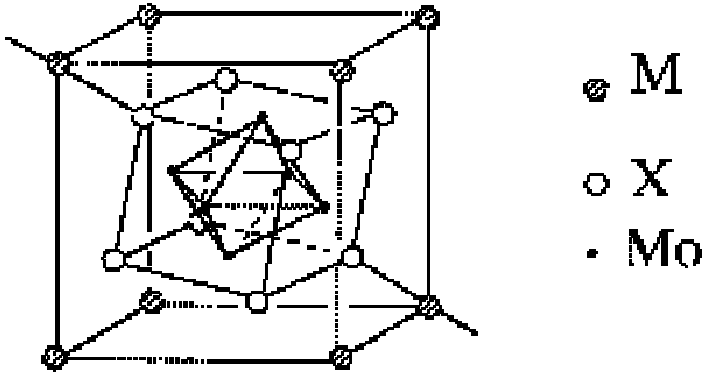

Figure 2. Elementary cell of rhombohedral structure

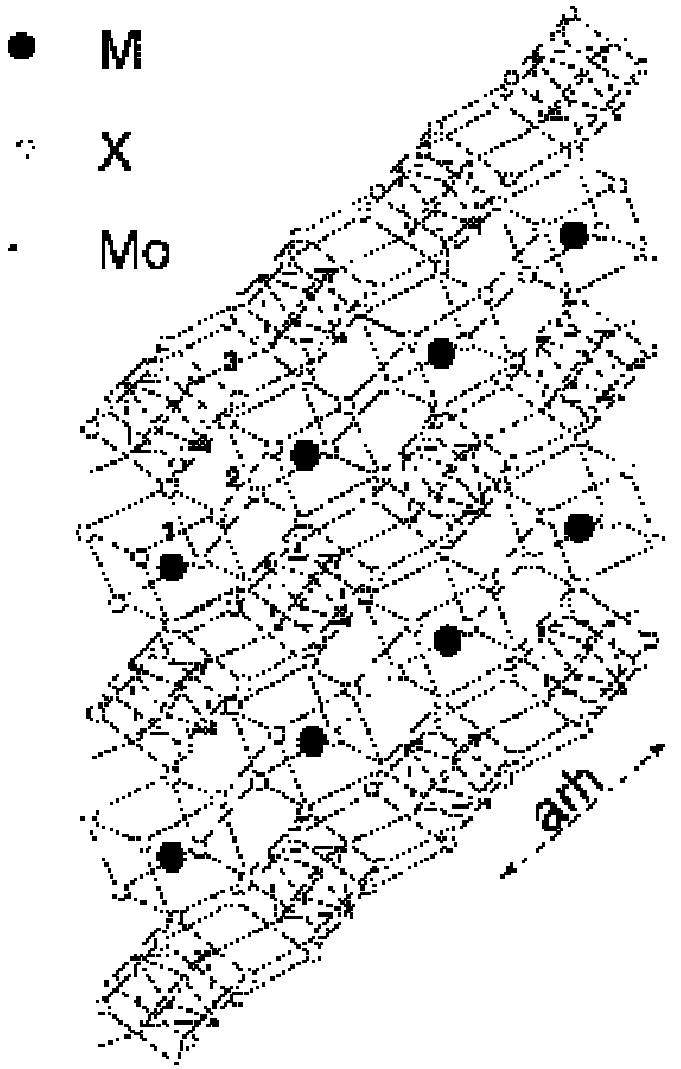

Figure 3. Projection on the hexagonal $(11\bar{2}0)$ plane. The three types of cavity are represented. Large cation are located in site 1.

Intercalation Reaction in Lithium Battery

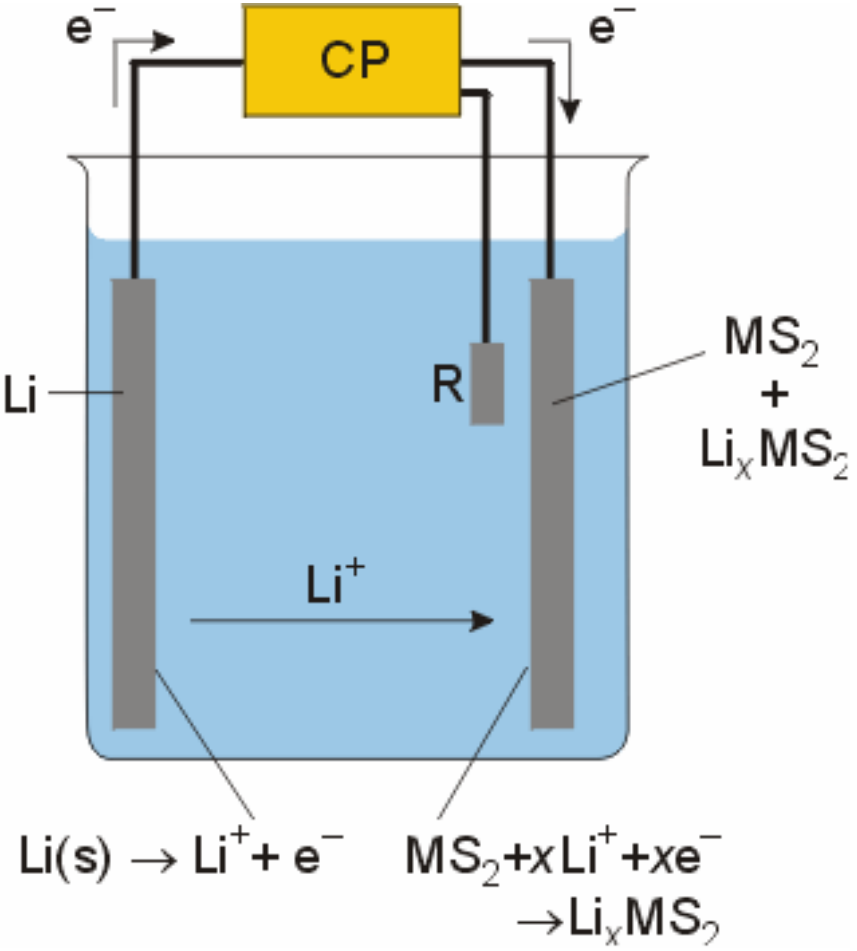

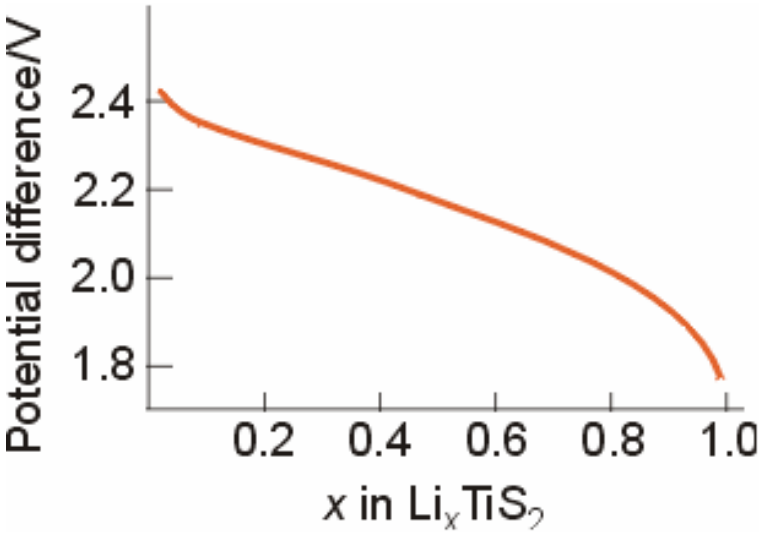

Glass formation

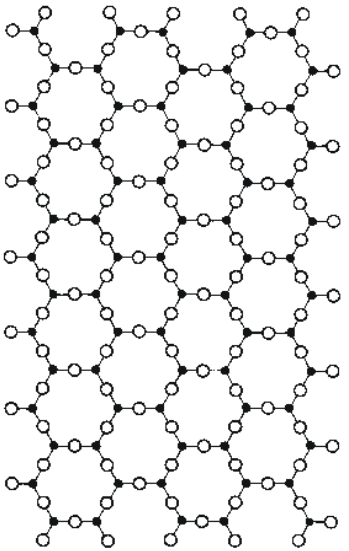

(a)

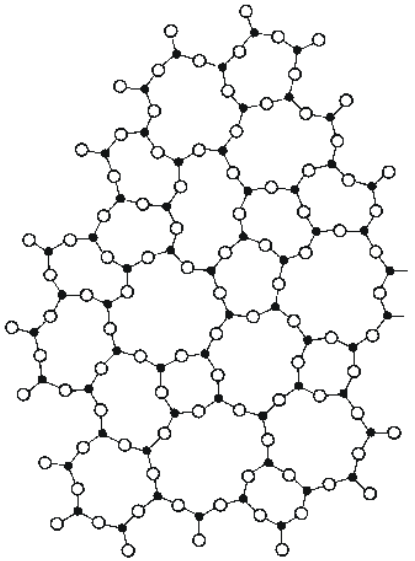

(b)

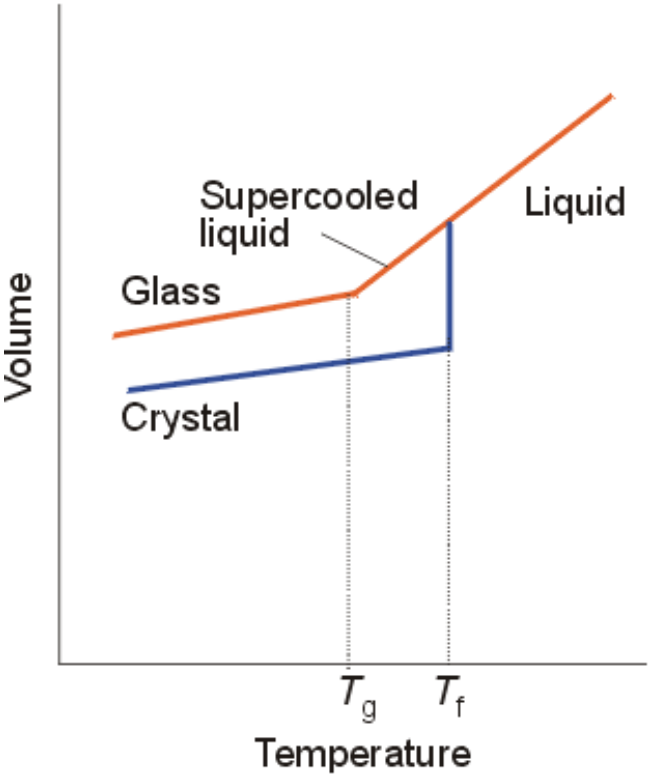

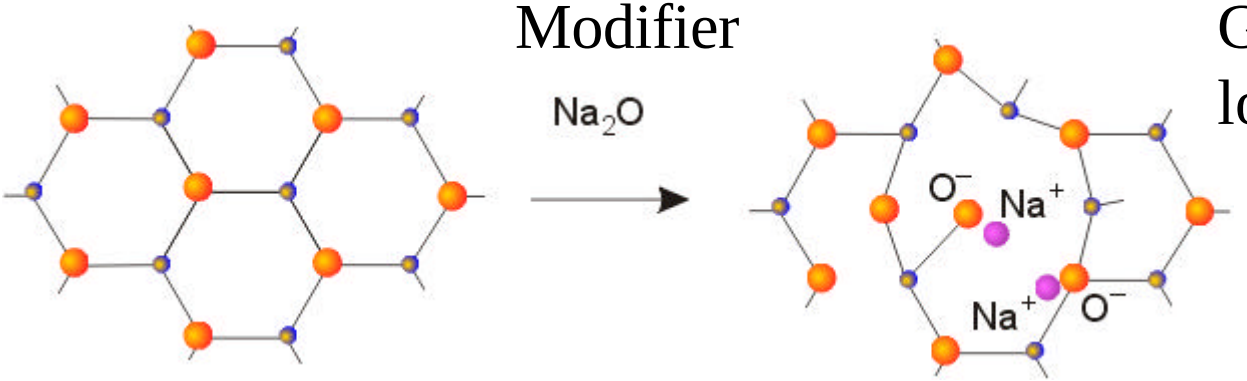

Glass of lower m.p.

18.29-31

Synthesis of Solid (Oxide) Materials by "Sol-Gel Method"

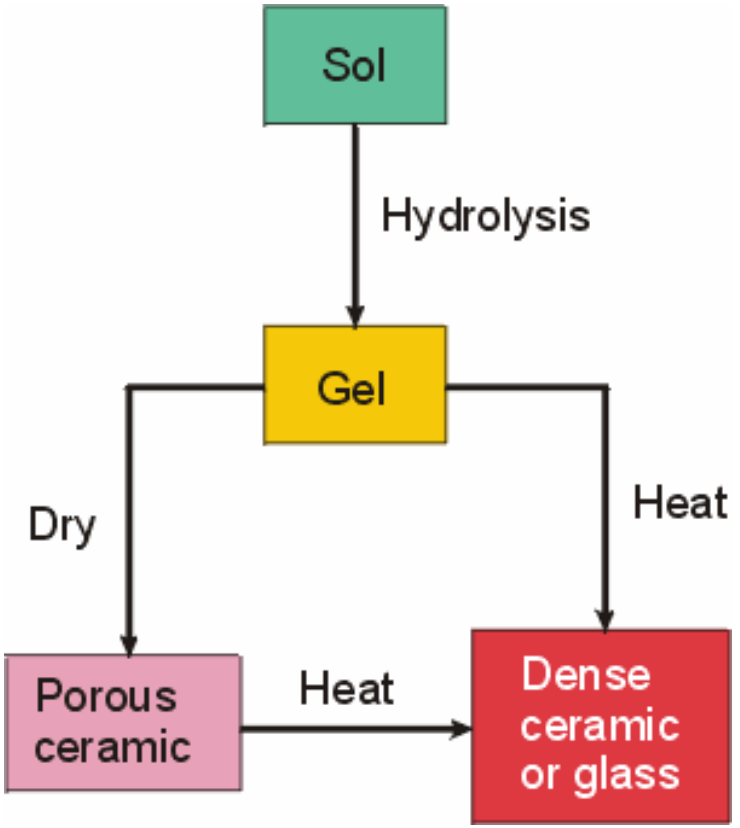

Chart18.1

Table 7.15 Some Metal Alkoxides Used for Sol–gel Processing of Ceramics

		Alkoxide
Single cation alkoxides		
I A (1) group	Li, Na	$LiOCH_3$ (s), $NaOCH_3$ (s)
I B (11) grp.	Cu	$Cu(OCH_3)_2$ (s)
II A (2) grp.	Ca, Sr, Ba	$Ca(OCH_3)_2$ (s) $Sr(OC_2H_5)_2$, $Ba(OC_2H_5)_2$ (s)
II B (12) grp.	Zn	$Zn(OC_2H_5)_2$ (s)
III A (3) grp.	B, Al, Ga	$B(OCH_3)_3$(l) $Al(i-OC_3H_7)_3$ (s) $Ga(OC_2H_5)_3$ (s)
III B (13) grp.	Y	$Y(OC_4H_9)_3$
IV A (4) grp.	Si, Ge	$Si(OC_2H_5)_4$ (l) $Ge(OC_2H_5)_4$ (l)
IV B (14) grp.	Pb	$Pb(OC_4H_9)_4$ (s)
V A (5) grp.	P, Sb	$P(OCH_3)_3$ (l) $Sb(OC_2H_5)_3$ (l)
V B (15) grp.	V, Ta	$VO(OC_2H_5)_3$ (l) $Ta(OC_3H_7)_5$ (l)
VI B (16) grp.	W	$W(OC_2H_5)_6$ (s)
lanthanide	La, Nd	$La(OC_3H_7)_3$ (s) $Nd(OC_2H_5)_3$ (s)
Alkoxides with various alkoxyl groups		
	Si	$Si(OCH_3)_4$ (l) $Si(OC_2H_5)_4$ (l) $Si(i-OC_3H_7)_4$ (l) $Si(t-OC_4H_9)_4$
	Ti	$Ti(OCH_3)_4$ (s) $Ti(OC_2H_5)_4$ (l) $Ti(i-OC_3H_7)_4$ (l) $Ti(OC_4H_9)_4$ (l)
	Zr	$Zr(OCH_3)_4$ (s) $Zr(OC_2H_5)_4$ (s) $Zr(OC_3H_7)_4$ (s) $Zr(OC_4H_9)_4$ (s)
	Al	$Al(OCH_3)_3$ (s) $Al(OC_2H_5)_3$ (s) $Al(i-OC_3H_7)_3$ (s) $Al(OC_4H_9)_3$ (s)
Double cation alkoxides		
	La-Al	$La[Al(i-OC_3H_7)_4]_3$
	Mg-Al	$Mg[Al(i-OC_3H_7)_4]_2$, $Mg[Al(s-OC_4H_9)_4]_2$
	Ni-Al	$Ni[Al(i-OC_3H_7)_4]_2$
	Zr-Al	$(C_3H_7O)_2Zr[Al(OC_3H_7)_4]_2$
	Ba-Zr	$Ba[Zr_2(OC_2H_5)_9]_2$

Source: H. Yanagida, K. Koumoto, and M. Miyayama, *The Chemistry of Ceramics*. Copyright © 1996 by

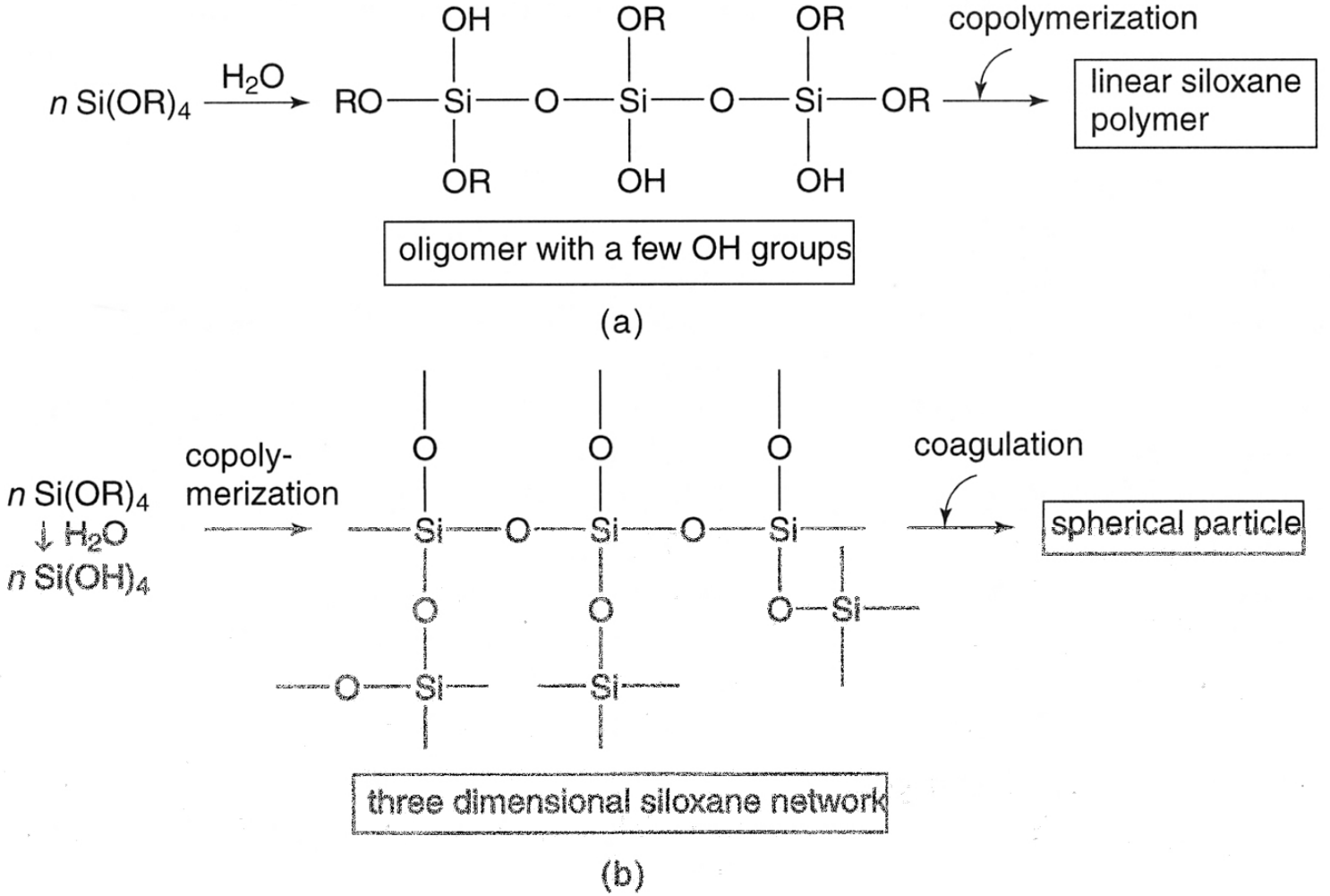

Figure 7.53 Hydrolysis and polymerization of a generic alkoxide $Si(OR)_4$ involving both (a) acid and (b) basic routes. Reprinted, by permission, from H. Yanagida, K. Koumoto, and M. Miyayama, *The Chemistry of Ceramics*, p. 148. Copyright © 1996 by John Wiley & Sons, Inc.

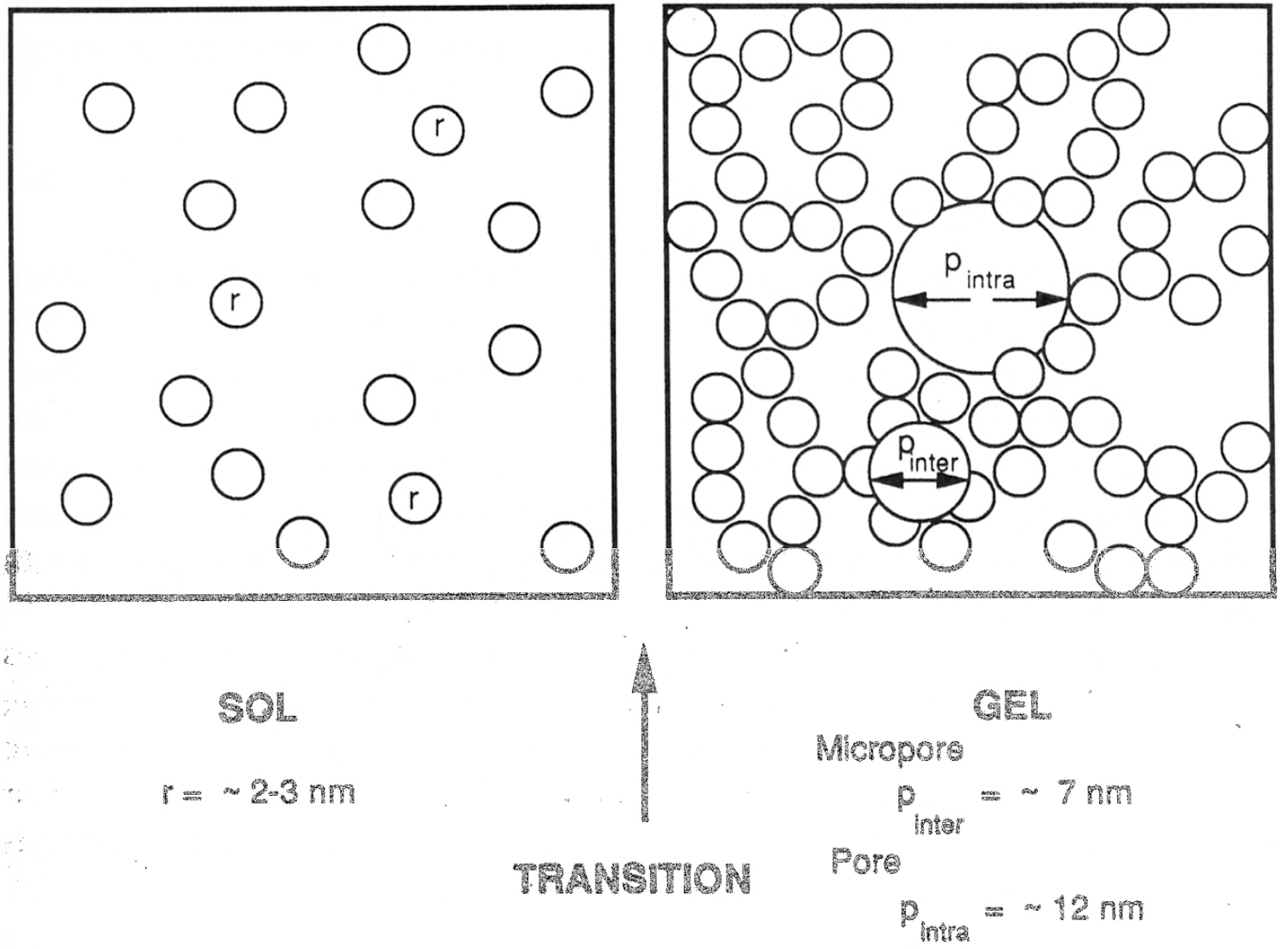

Figure 7.3. Schematic diagram of the linked particles of a dried gel following the colloidal route.

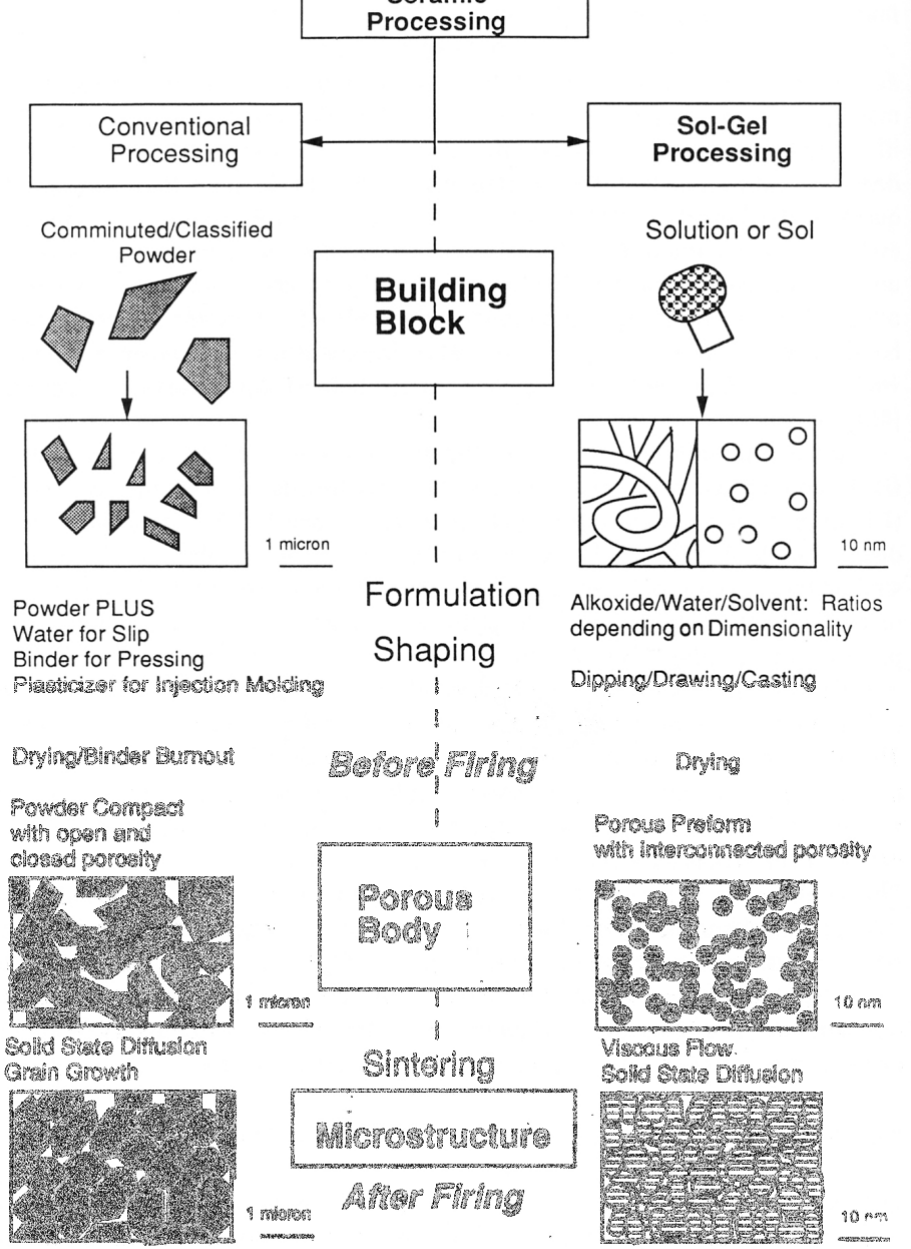

Figure 7.5. Comparison of steps in conventional processing of ceramics with those in

Superconductor

- Zero electrical resistance at temperatures below critical temperature
- Superconducting phase transition
- Meissner effect

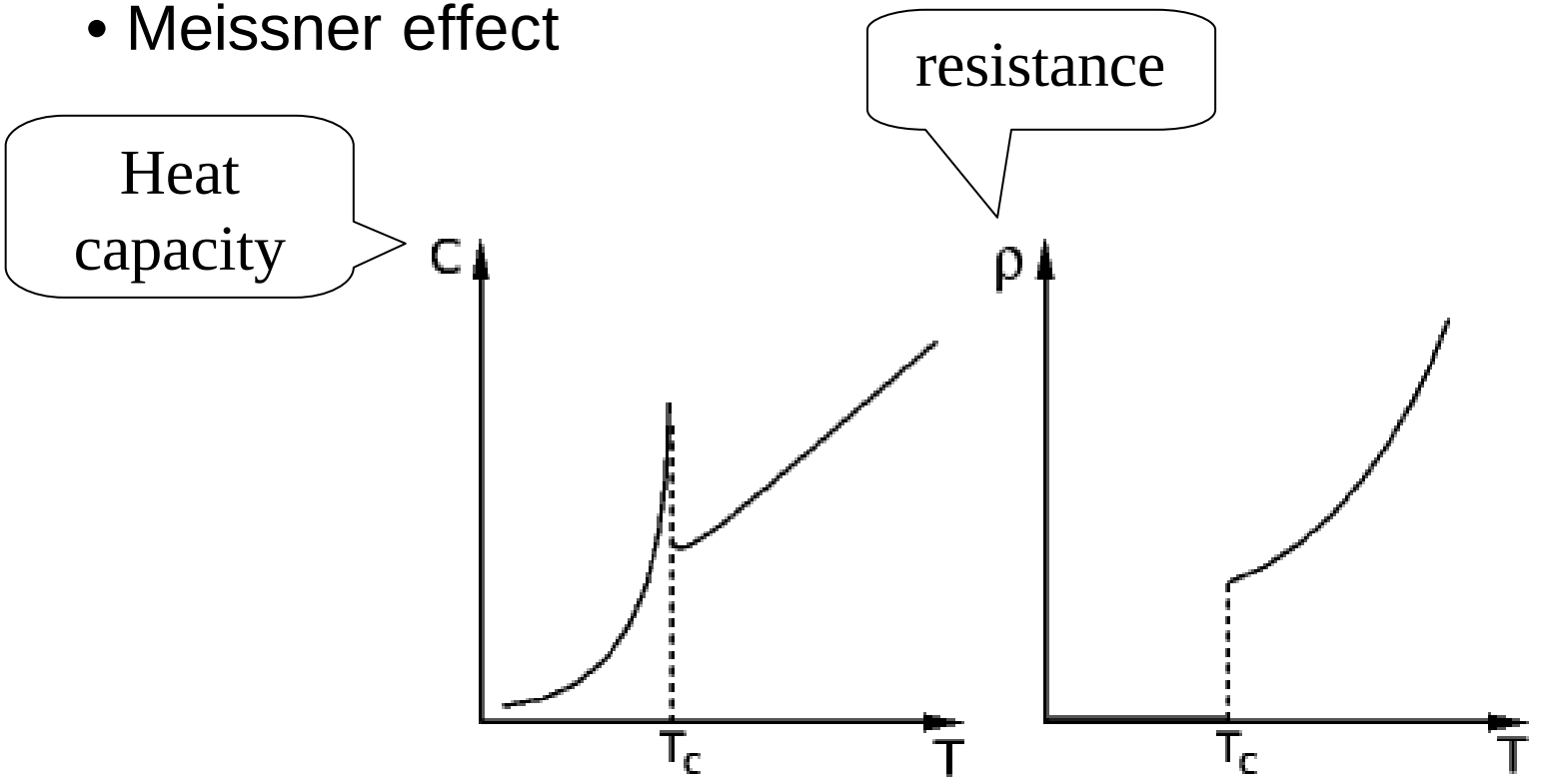

Meissner effect with high temp. superconductor
Photo from Pacific Northwest National Laboratory

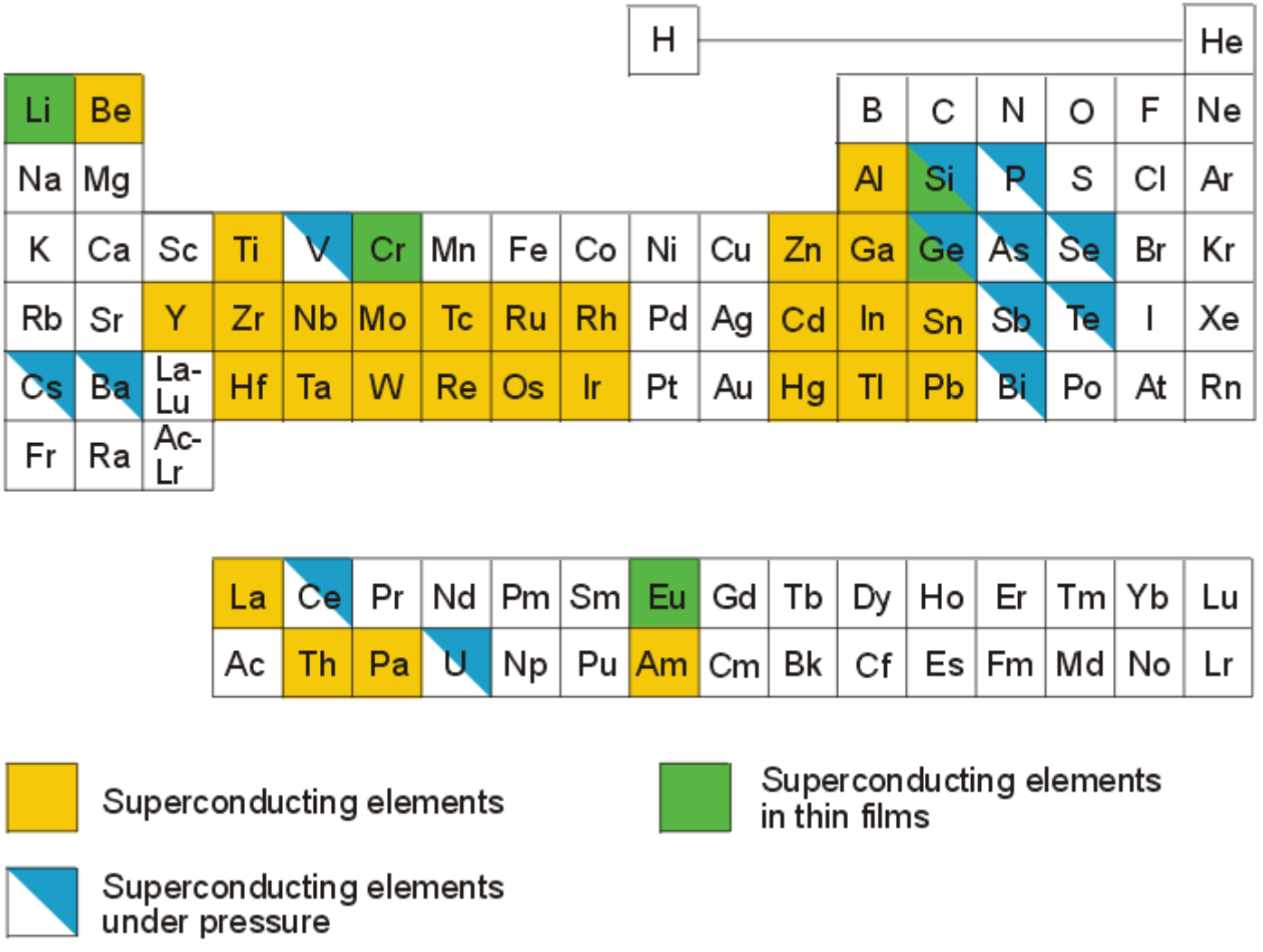
H
He
Li
Be
B
C
N
O
F
Ne
Na
Mg
Al
Si
P
S
Cl
Ar
K
Ca
Sc
Ti
V
Cr
Mn
Fe
Co
Ni
Cu
Zn
Ga
Ge
As
Se
Br
Kr
Rb
Sr
Y
Zr
Nb
Mo
Tc
Ru
Rh
Pd
Ag
Cd
In
Sn
Sb
Te
I
Xe
Cs
Ba
La-Lu
Hf
Ta
W
Re
Os
Ir
Pt
Au
Hg
Tl
Pb
Bi
Po
At
Rn
Fr
Ra
Ac-Lr
La
Ce
Pr
Nd
Pm
Sm
Eu
Gd
Tb
Dy
Ho
Er
Tm
Yb
Lu
Ac
Th
Pa
U
Np
Pu
Am
Cm
Bk
Cf
Es
Fm
Md
No
Lr
Superconducting elements
Superconducting elements in thin films
Superconducting elements under pressure

Table 18.4 Some superconductors

Elements	T_c/K	Compounds	T_c/K
Zn	0.88	Nb_3Ge	23.2
Cd	0.56	Nb_3Sn	18.0
Hg	4.15	$LiTiO_4$	13
Pb	7.19	$K_{0.4}Ba_{0.6}BiO_3$	29.8
Nb	9.50	$YBa_2Cu_3O_7$	95
		$Tl_2Ba_2Ca_2Cu_3O_{10}$	122

High temperature superconductor

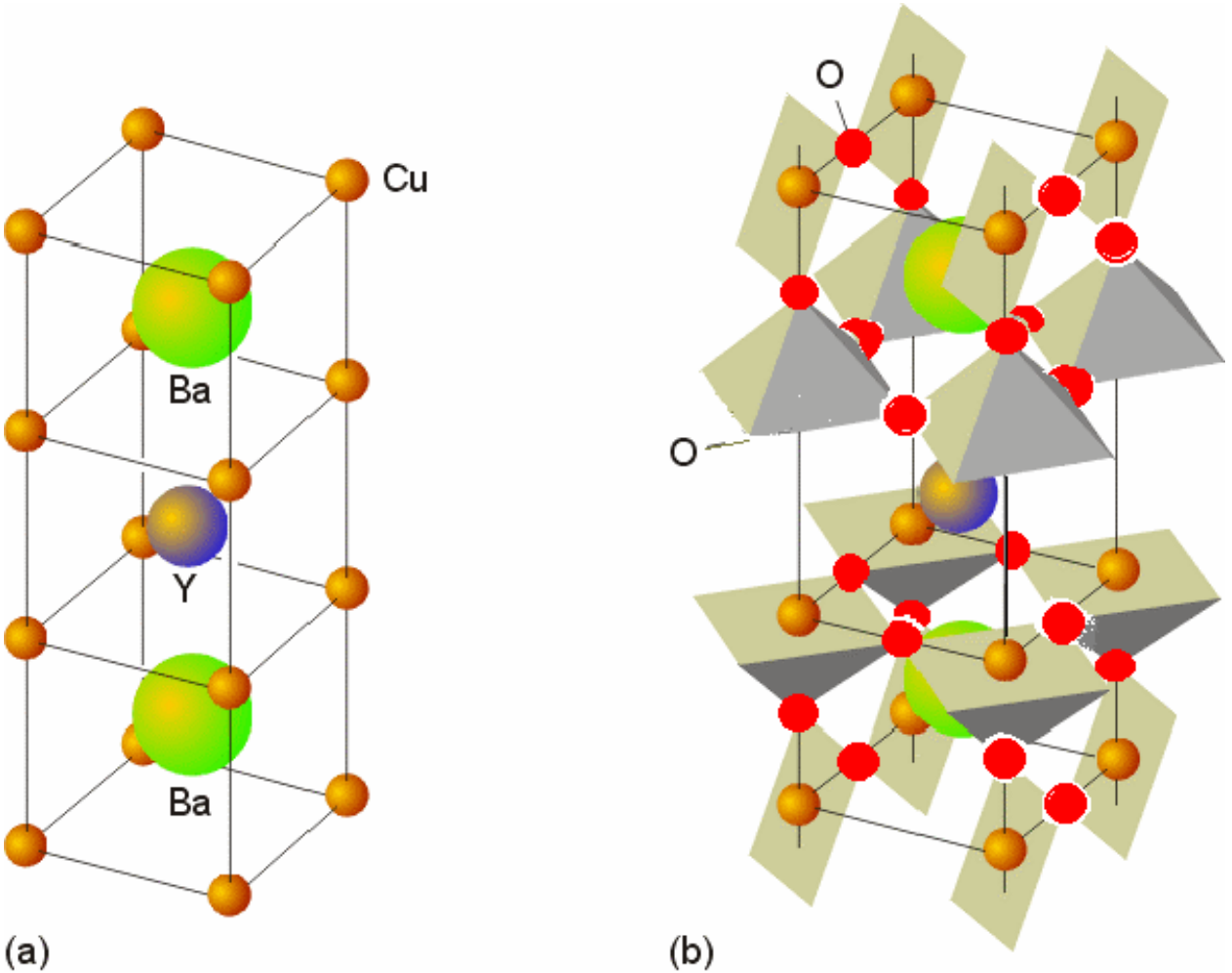

$YBa_2Cu_3O_7$

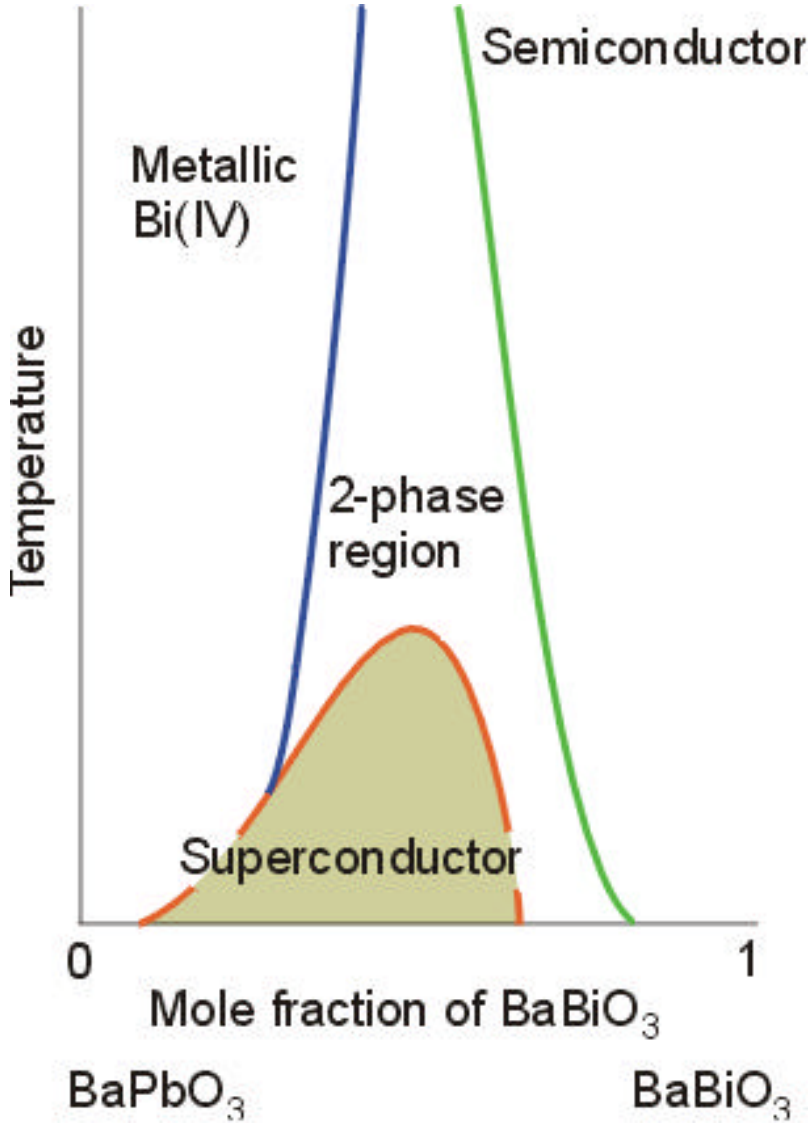

Superconductivity is usually observed for materials that are not highly conducting above the critical temperature.

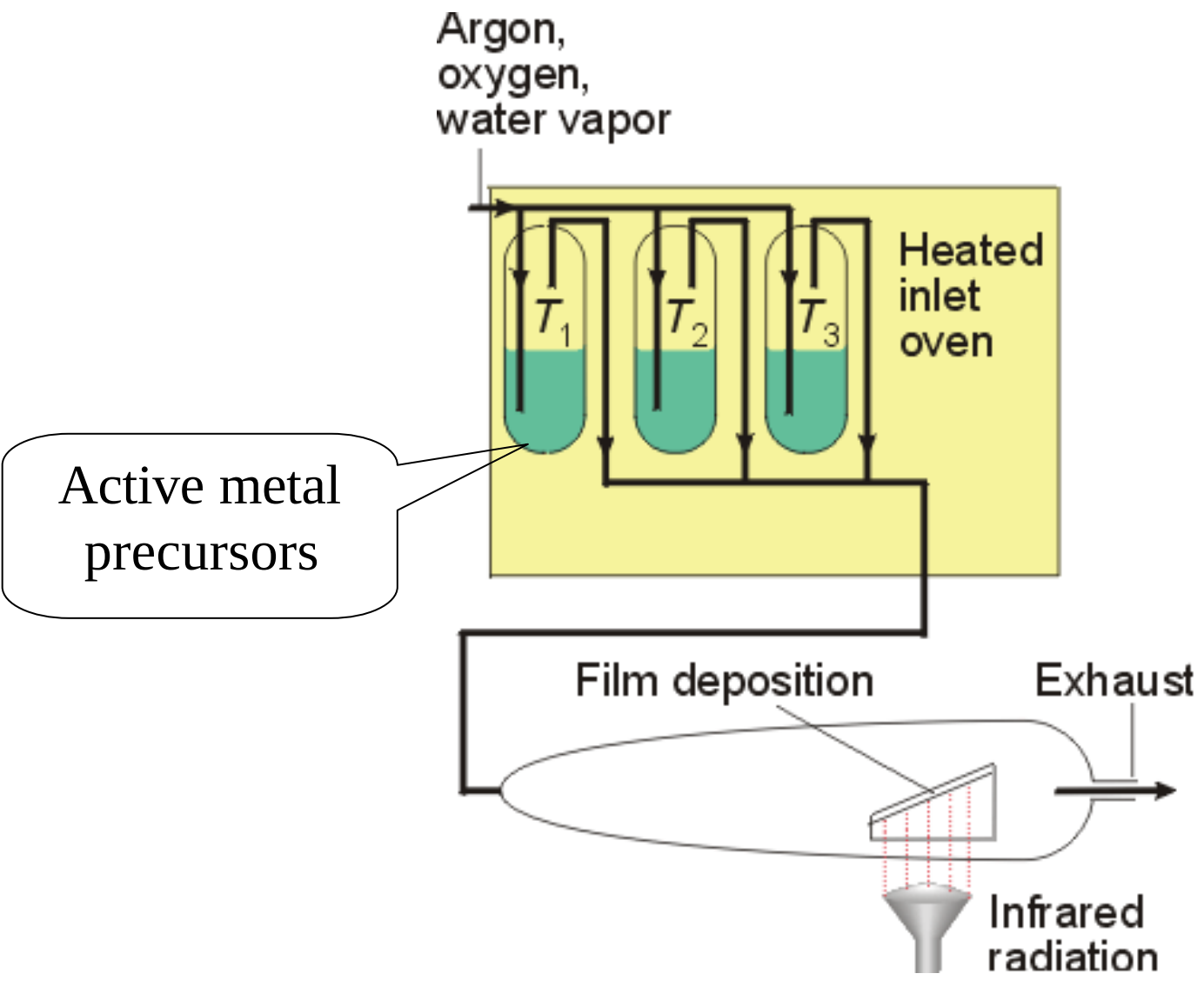

Chemical vapor deposition (CVD) of superconductor thin film.

Buckyball

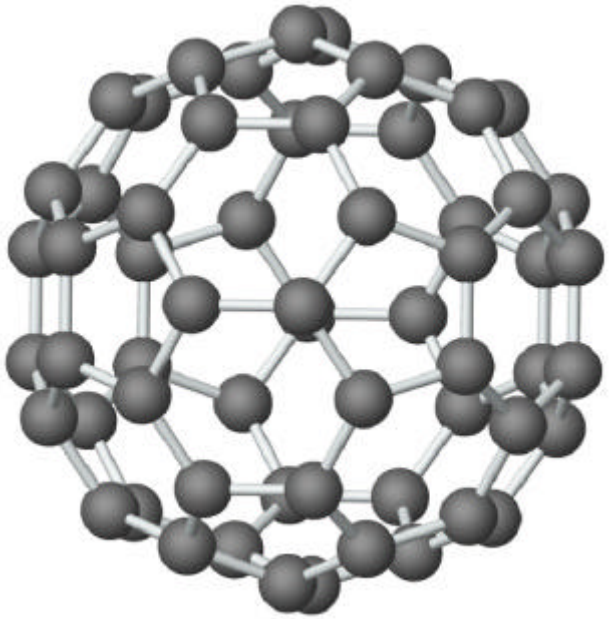

Table 6.3 Physical constants for C_{60}[b]

Quantity	*Value*	*Quantity*	*Value*
Average C—C distance	144 pm	Band gap (HOMO–LUMO)	1.7 eV
fcc Lattice constant	1417 pm	Binding energy per atom	7.40 eV
C_{60} mean ball diameter	683 pm	Debye temperature	185 K
C_{60} ball outer diameter[a]	1018 pm	Thermal conductivity (300 K)	0.4 W/mK
C_{60} ball inner diameter[a]	348 pm	Phonon mean free path	5000 pm
Tetrahedral site radius	112 pm	Static dielectric constant	4.0–4.5
Octahedral site radius	207 pm	Velocity of sound v_t	2.1×10^5 cm/sec
Electron affinity (pristine C_{60})	2.65 eV	Structural phase transitions	255 K, 165 K
Ionization energy (first)	7.58 eV	Mass density	1.72 g/cm^3
Ionization energy (second)	11.5 eV		

[a] The inner and outer diameters of the C_{60} molecule are estimated from (683 − 335 pm) and (683 + 335 pm), respectively, where 335 pm is the interlayer spacing in graphite.

[b] From the compilation of M. S. Dresselhaus, G. Dresselhaus, and P. C. Eklund, *J. Mater Res.* **1993,** *8,* 2054. Original references given in source.

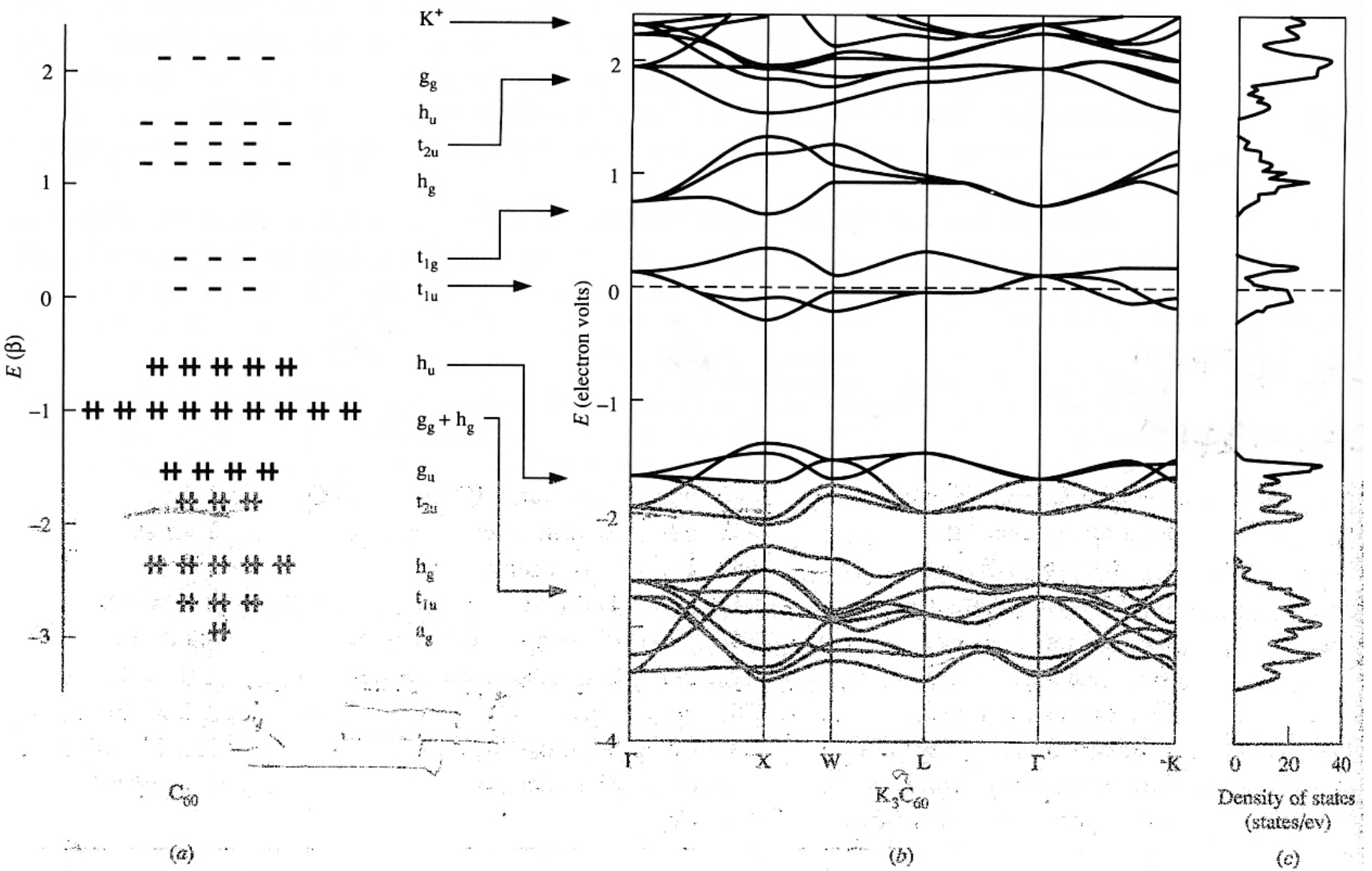

Figure 6.37 (*a*) Molecular orbitals of C_{60}. (*b*) Band structure of K_3C_{60}. (*c*) Corresponding density-of-states curves. (From A. F. Hebard, Physics Today, Nov. 1992, 29.)

Electron-doped C60

Na, K, Rb, Cs-doped C60: Tc~ 16-18 K

Hole-doped C60

C60/$CHBr_3$: *T*c ~ 52 K

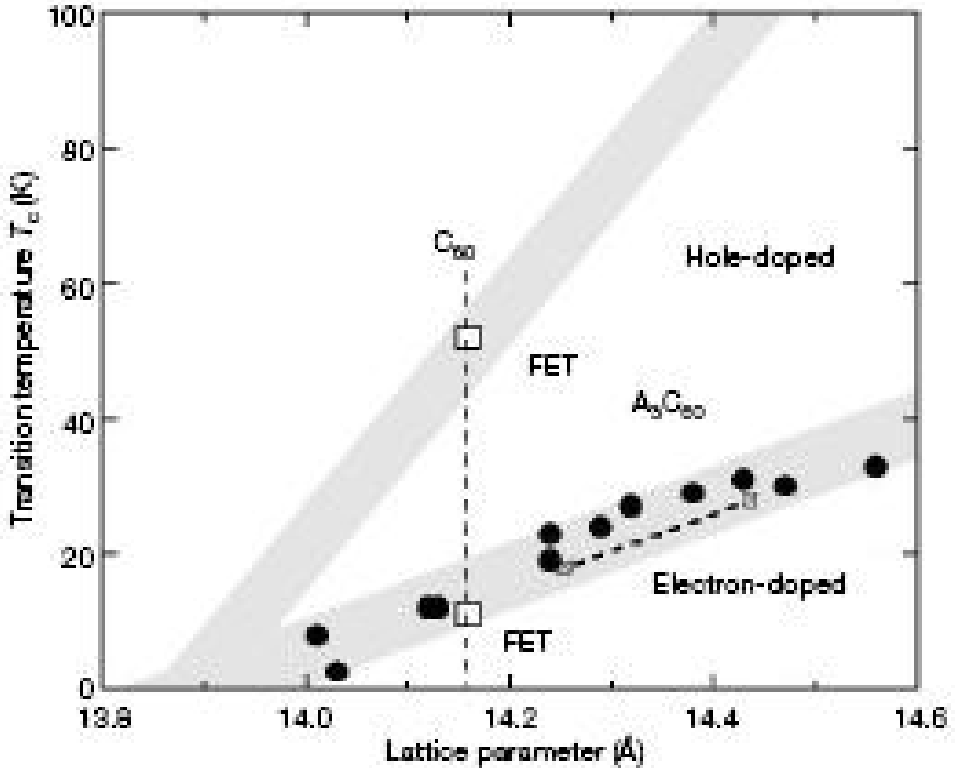

Figure 7. Transition temperature in electron- and hole-doped C60 as function of lattice parameter.

Nature, 408 (2000) 549

Crystallographic Space Group

230 space group types into 32 crystal classes, one for each associated crystallographic point group.
The space groups within each crystal class are characterized by the 14 Bravais lattices which belong to one of 7 crystal systems.

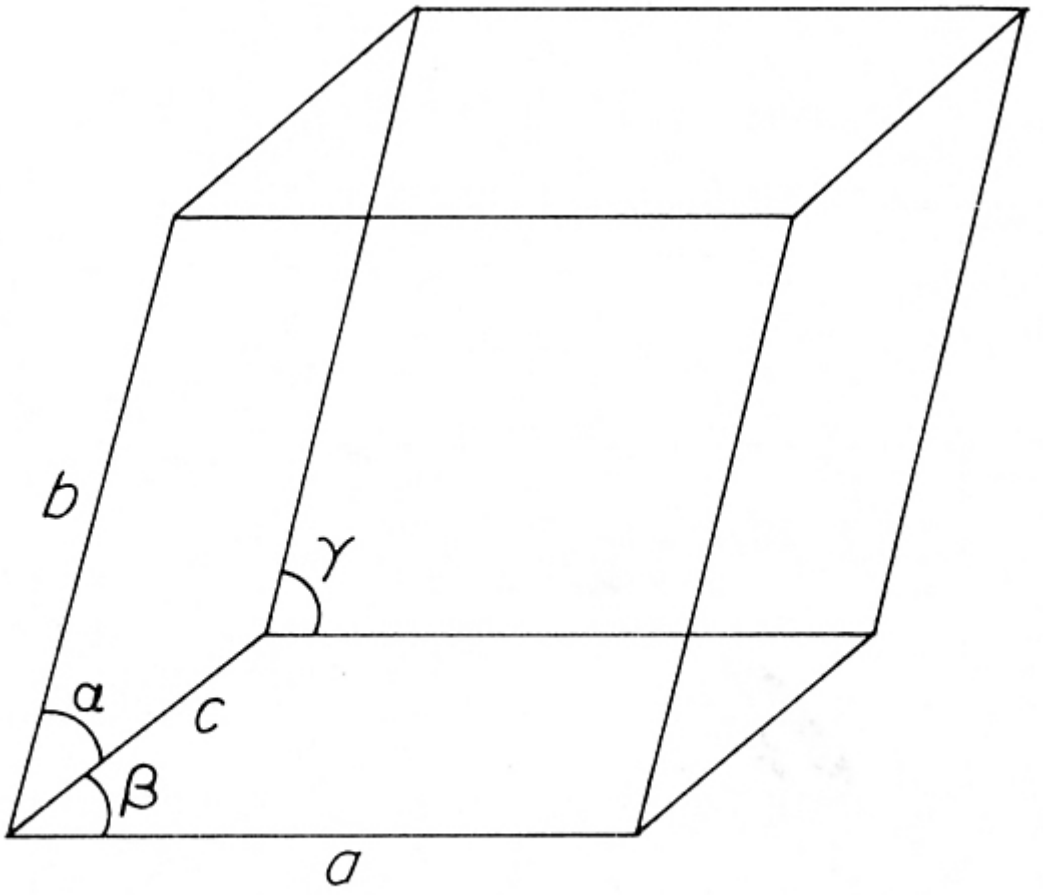

Fig. 1.5a. *Unit cell parameters*

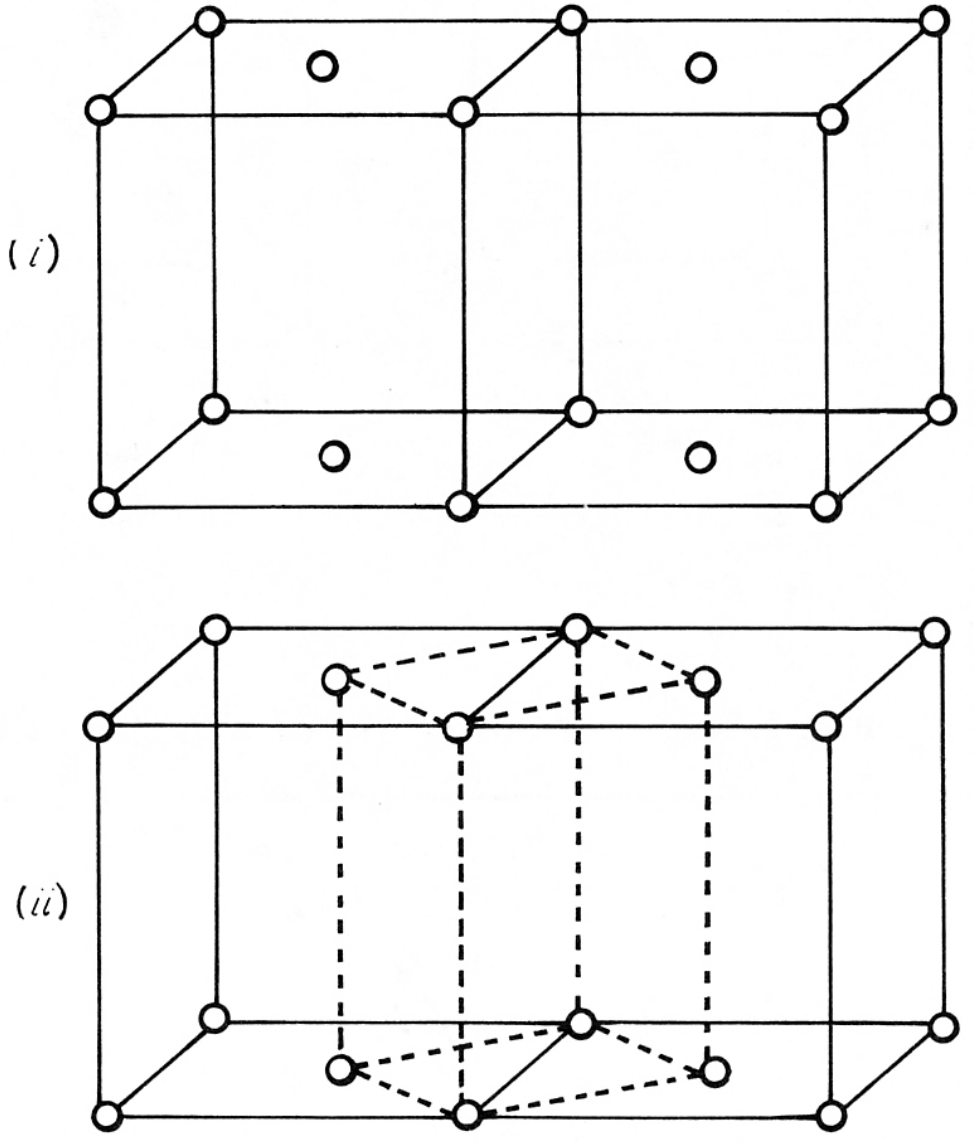

Fig. 1.5d. *Correct choice of unit cell*

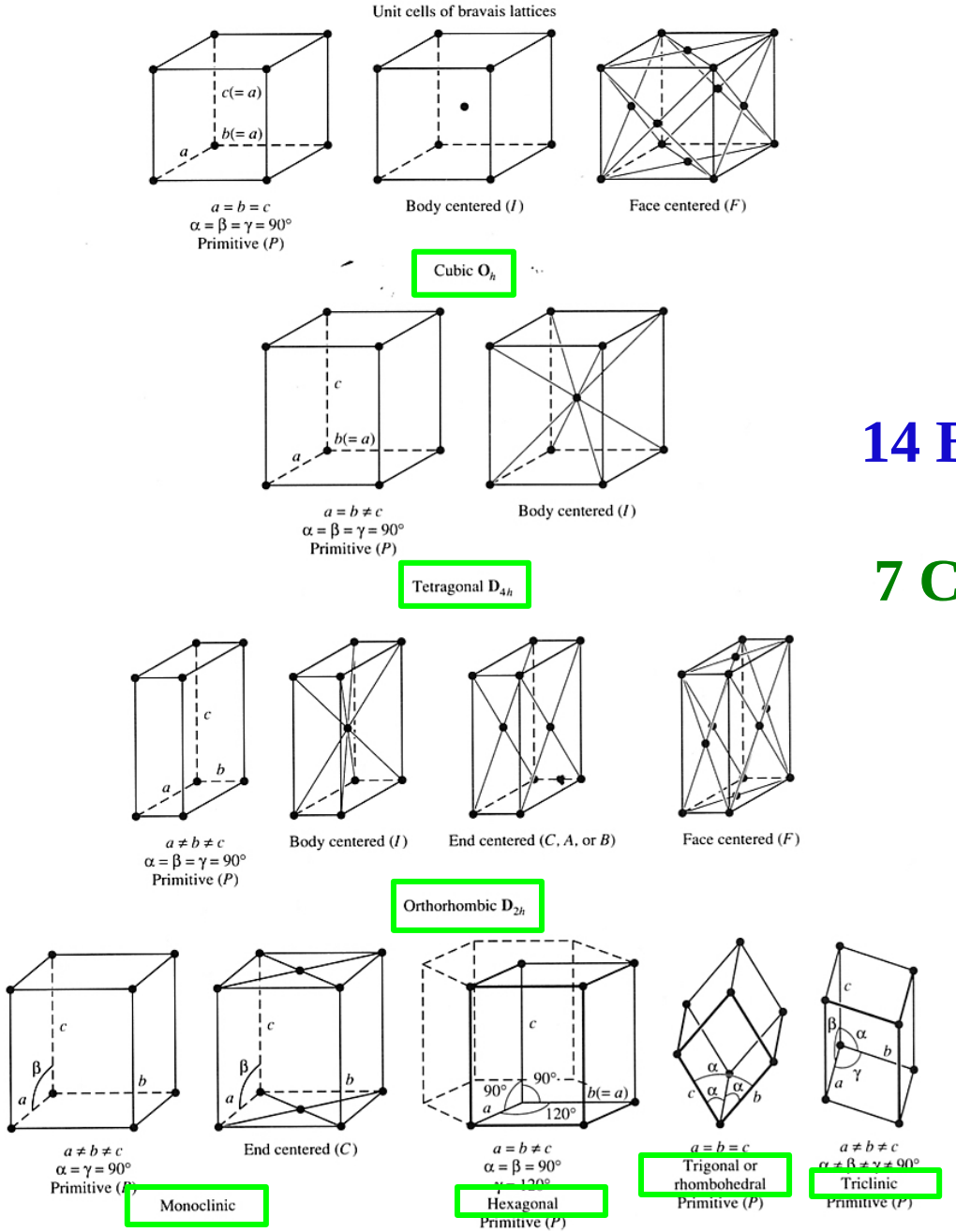

14 Bravais Lattice

7 Crystal Systems

Schöenflies Notation

Hermann-Mauguin Notation

Table 6.1 Crystal systems

Name	*Point group of lattice*		*Unit cell*	*Subgroups*		*Order*
Triclinic	$C_i(S_2)$	$\bar{1}$	$a \neq b \neq c$ $\alpha \neq \beta \neq \gamma \neq 90°$	C_1 C_i	1 $\bar{1}$	1 2
Monoclinic	C_{2h}	$2/m$	$a \neq b \neq c$ $\alpha = \gamma = 90° \neq \beta$	C_{1h} C_2 C_{2h}	m 2 $2/m$	2 2 4
Orthorhombic	D_{2h}	mmm	$a \neq b \neq c$ $\alpha = \beta = \gamma = 90°$	C_{2v} D_2 D_{2h}	$mm2$ 222 mmm	4 4 8
Tetragonal	D_{4h}	$4/mmm$	$a = b \neq c$ $\alpha = \beta = \gamma = 90°$	C_4 S_4 C_{4h} D_{2d} C_{4v} D_4 D_{4h}	4 $\bar{4}$ $4/m$ $\bar{4}2m$ $4mm$ 422 $4/mm$	4 4 8 8 8 8 16
Trigonal (rhombohedral)	D_{3d}	$\bar{3}m$	$a = b = c$ $120° > \alpha = \beta = \gamma \neq 90°$	C_3 S_6 C_{3v} D_3 D_{3d}	3 $\bar{3}$ $3m$ 32 $\bar{3}m$	3 6 6 6 12
Hexagonal	D_{6h}	$6/mmm$	$a = b \neq c$ $\alpha = \beta = 90°$ $\gamma = 120°$	C_{3h} C_6 C_{6h} D_{3h} C_{6v} D_6 D_{6h}	$\bar{6}$ 6 $6/m$ $\bar{6}m2$ $6mm$ 622 $6/mmm$	6 6 12 12 12 12 24
Cubic	O_h	$m\bar{3}m$	$a = b = c$ $\alpha = \beta = \gamma = 90°$	T T_h T_d O O_h	23 $m\bar{3}$ $\bar{4}3m$ 432 $m\bar{3}m$	12 24 24 24 48

Miller Indices (hkl): a plane in the crystal lattice

h = a/cutting point along a-axis

k = b/cutting point along b-axis

l = c/ cutting point along c-axis

Miller Indices (hkl)

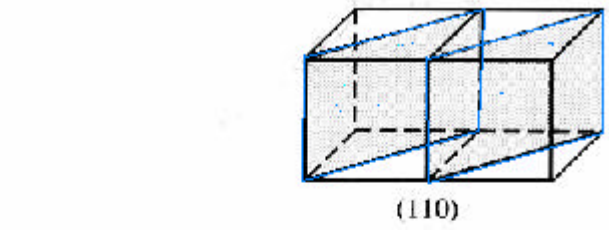

Face cutting
-1a and 1b

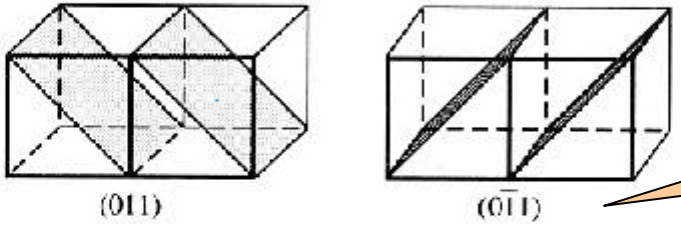

Face cutting
–1b and 1c

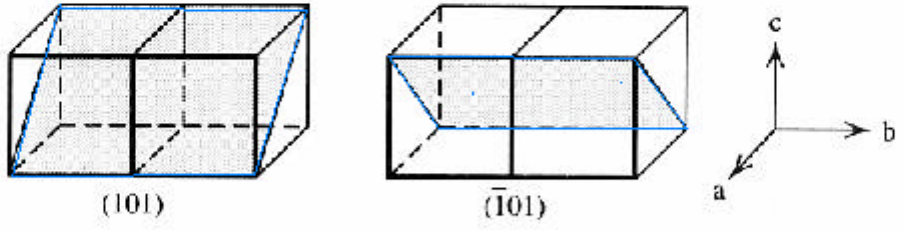

Face cutting
-1/2a, 1/2b
and 1/2c

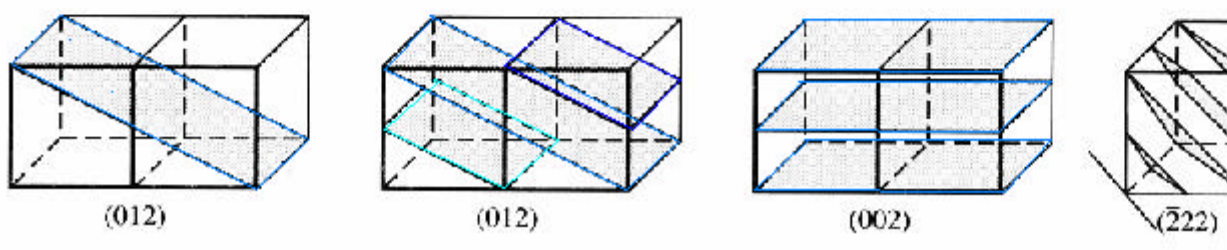

Figure 6.2 Miller indices. The [110] form and others as indicated.

Crystallographic data

34-268 ★

$CuY_2Si_4O_{12}$

Copper Yttrium Silicate

Rad. $CuK\alpha_1$ λ 1.54056 Filter Mono. d-sp Guinier
Cut off Int. Diffractometer $1/1_{cor.}$ 2.1
Ref. Lambert. Fysel. Mineralogisch-Petrographisches Institut. Universitat Heidelberg Germany. *JCPDS Grant-in-Aid Report.* (1983)

Sys. Monoclinic S.G. C */*
a 7.052 b 14.283 c 4.738 A 0.4937 C 0.3317
α β 103.32 γ Z 2
Ref.

D_x 3.902 D_m 3.980 mp

Color: Light-blue
CuO (p.a., Merck) + Y_2O_3 (puriss., Fluka) + $45iO_2$ (Aerosil, Degussa) heated for three weeks in open Pt-crucible at 1000 C. Space group from powder data. F_{30} = 81.5(0.009,42) Silicon used as internal standard. PSC: mC38

See following card

d Å	Int	hkl	d Å	Int	hkl
7.15	9	020	2.0427	16	241
6.19	20	110	1.9554	6	260,170
4.61	14	001	1.9366	4	042
4.13	14	111	1.8925	4	261
3.873	40	021	1.8668	1	311
3.434	4	200	1.8465	14	242
3.375	55	111	1.8348	4	312
3.118	100	201	1.8171	5	152
3.094	20	220	1.7858	9	350,080
2.823	80	041	1.7764	9	$\bar{3}51$
2.806	25	1.31	1.7444	2	$\bar{4}01$
2.637	25	150	1.7371	10	202
2.491	14	201	1.7156	10	400
2.473	30	240	1.6854	6	421
2.382	3	151,060	1.6677	3	222
2.362	10	221	1.6585	4	420
2.323	5	$\bar{1}12$	1.6538	19	152
2.306	9	002	1.5984	2	352
2.259	8	310	1.5841	2	280
2.240	12	$\bar{3}11$	1.5727	9	351
2.206	23	151	1.5675	12	$\bar{4}41$
2.193	5	022	1.5622	12	242
2.157	10	202	1.5585	14	402
2.115	3	061	1.5531	3	352
2.0636	8	$\bar{2}22$	1.5467	12	440,190

Diffraction Pattern

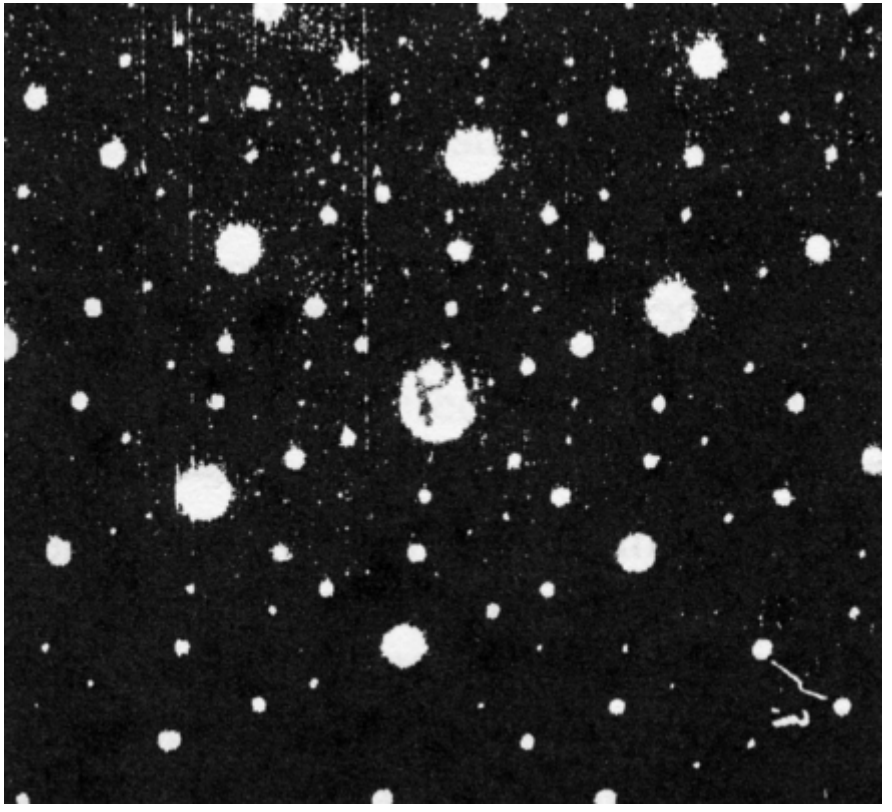

<Ref> Structure determination by X-ray crystallography
M.F.C. Ladd and R.A. Palmer, NY : Plenum Press, 1985.

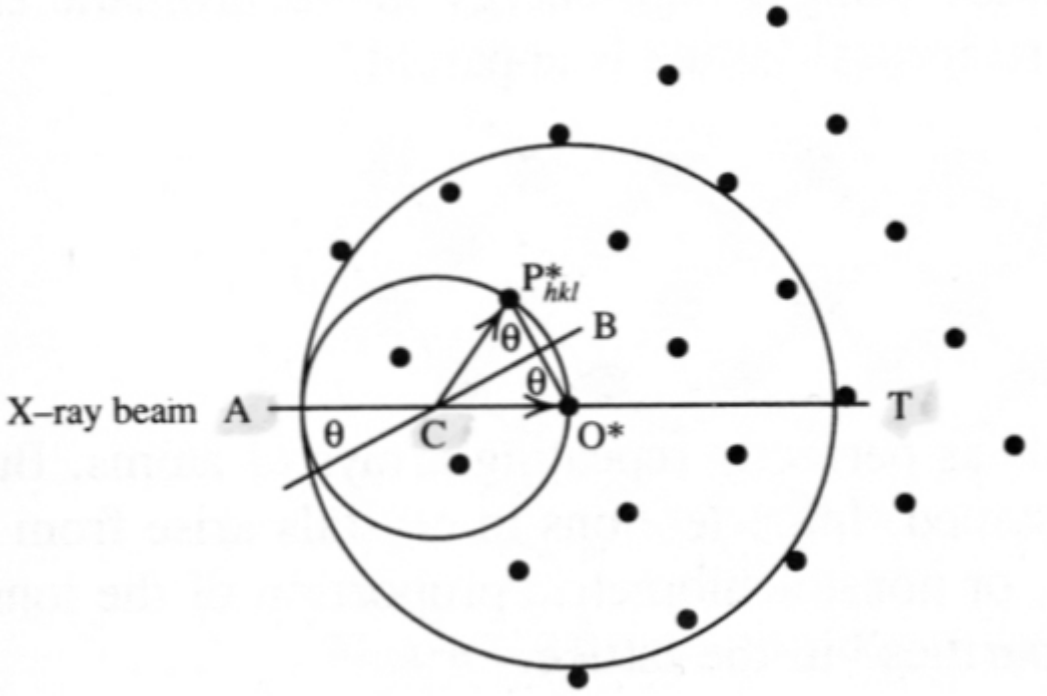

2dsin q **= n** l

sin q **= n** l **/2 (1/d)** ⟹ Reciprocal lattice

real space ($\vec{a}$, $\vec{b}$, $\vec{c}$) ? reciprocal space ($\vec{a}*$, $\vec{b}*$, $\vec{c}*$)

The non-coplanar vectors $\vec{a}$, $\vec{b}$, and $\vec{c}$ define a unit cell in the real lattice. The corresponding vectors for the unit cell of a reciprocal lattice $\vec{a}*$, $\vec{b}*$, and $\vec{c}*$ will be defined by

$$\vec{a}* = \frac{1}{\vec{a}} = \frac{\vec{c}\times\vec{b}}{V} \qquad \vec{b}* = \frac{1}{\vec{b}} = \frac{\vec{c}\times\vec{a}}{V} \qquad \vec{c}* = \frac{1}{\vec{c}} = \frac{\vec{a}\times\vec{b}}{V}$$

where the unit cell volume V is given by

$$V = \vec{a}\times\vec{b}\times\vec{c} = 1/V^*$$

Hence, the reciprocal lattice vectors, and are normal to the planes **bc**, **ca**,and **ab** respectively in the real space. By the way, the symmetry in the reciprocal space is the same as in the real space.

Relation of the Crystal lattice and

Reciprocal lattice

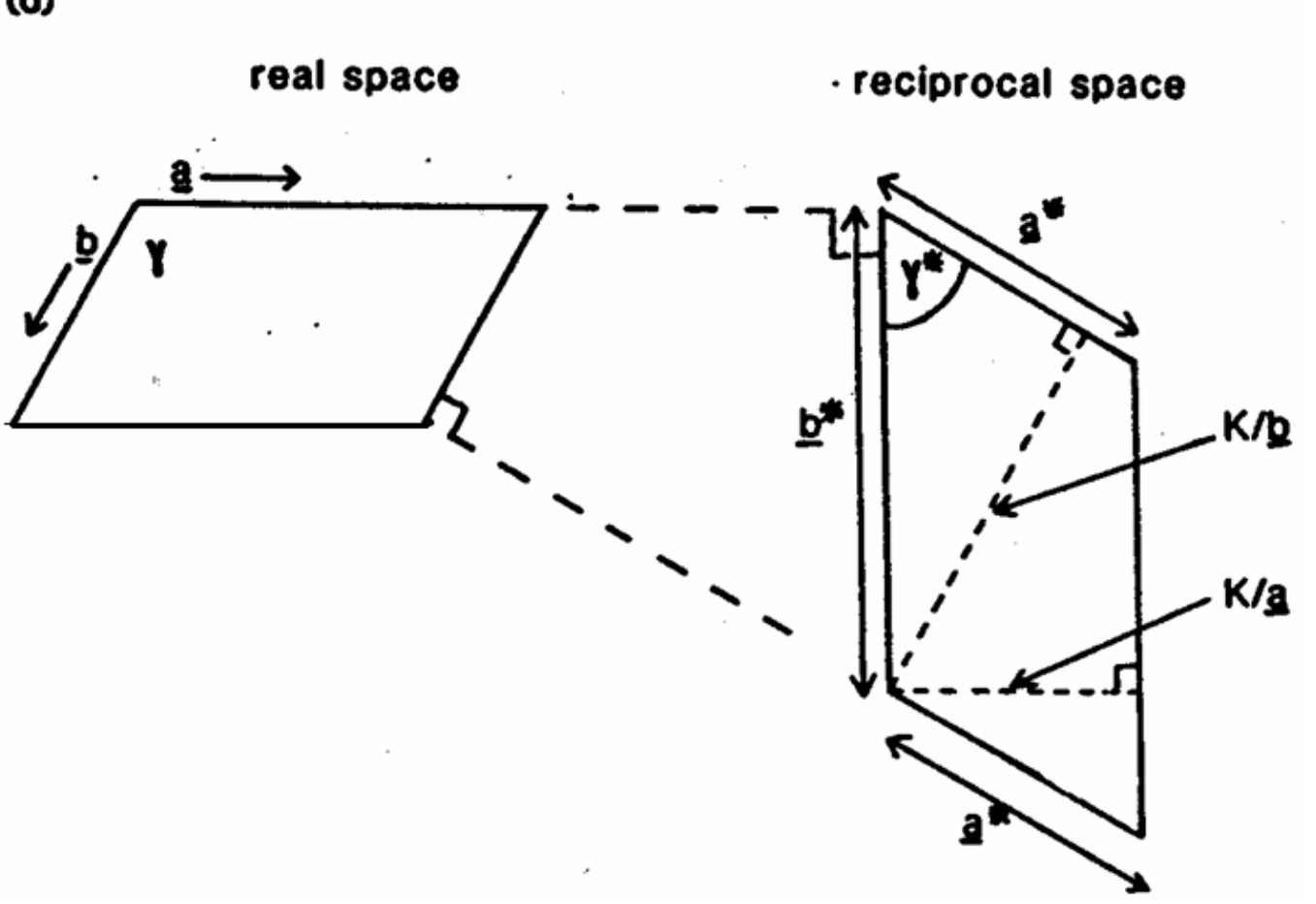

Reciprocal lattice

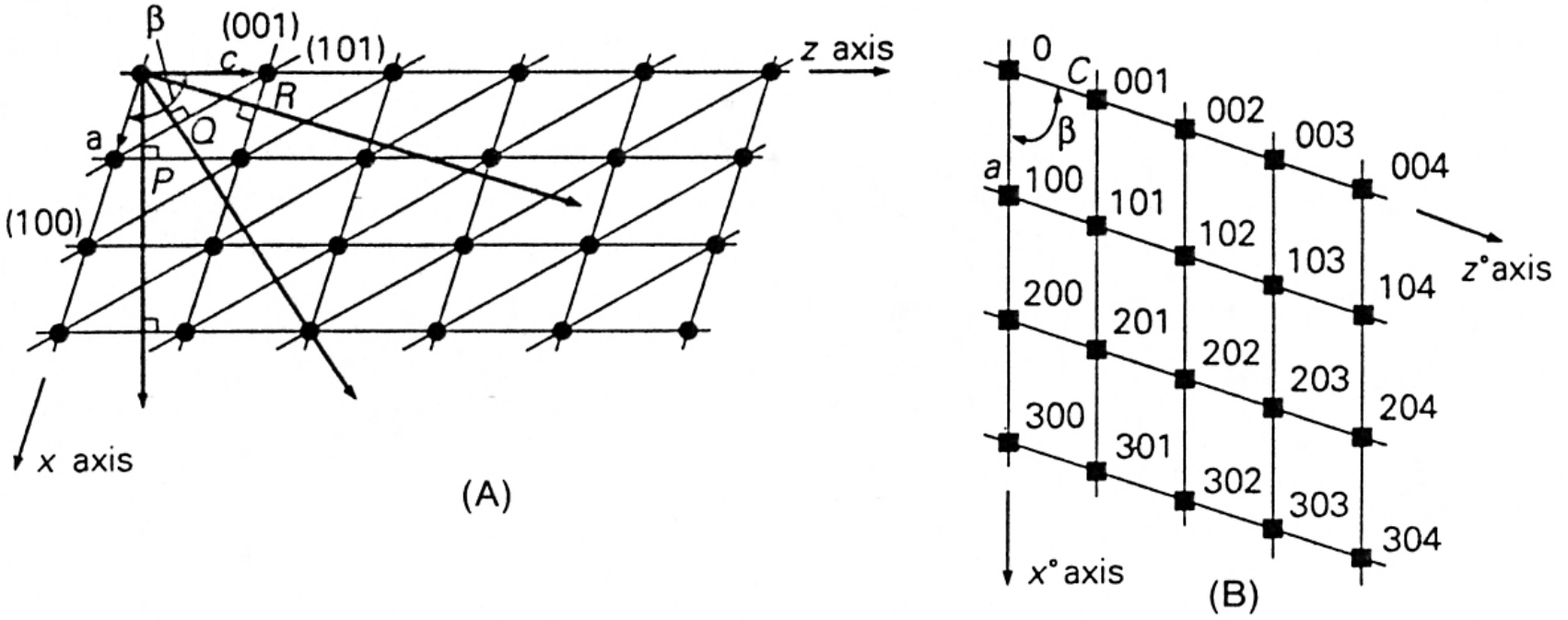

FIGURE 17–2 (A) Direct and (B) reciprocal lattices. (Reproduced with permission from M. F. C. Ladd and R. A. Palmer, "Structure Determination by X-Ray Crystallography." 2nd ed. Plenum Press, New York.)

Stereographic projection

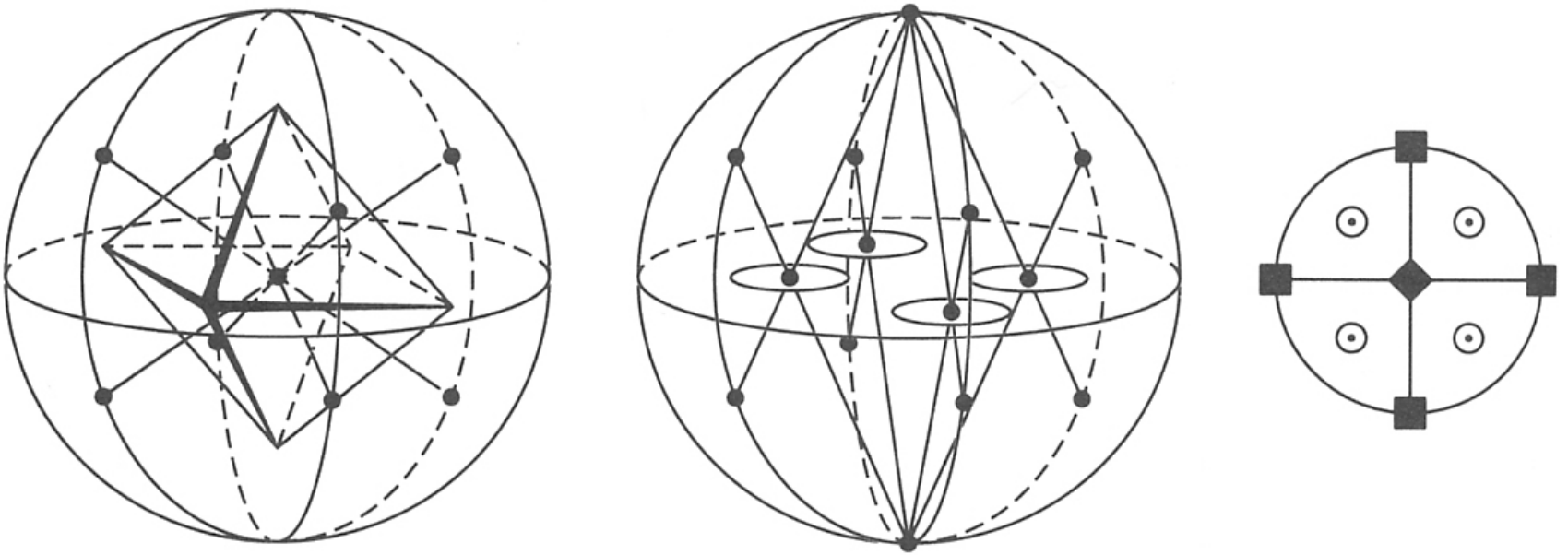

Figure 6.3 Construction of stereographic projection of an octahedron.

Conventional graphic symbols

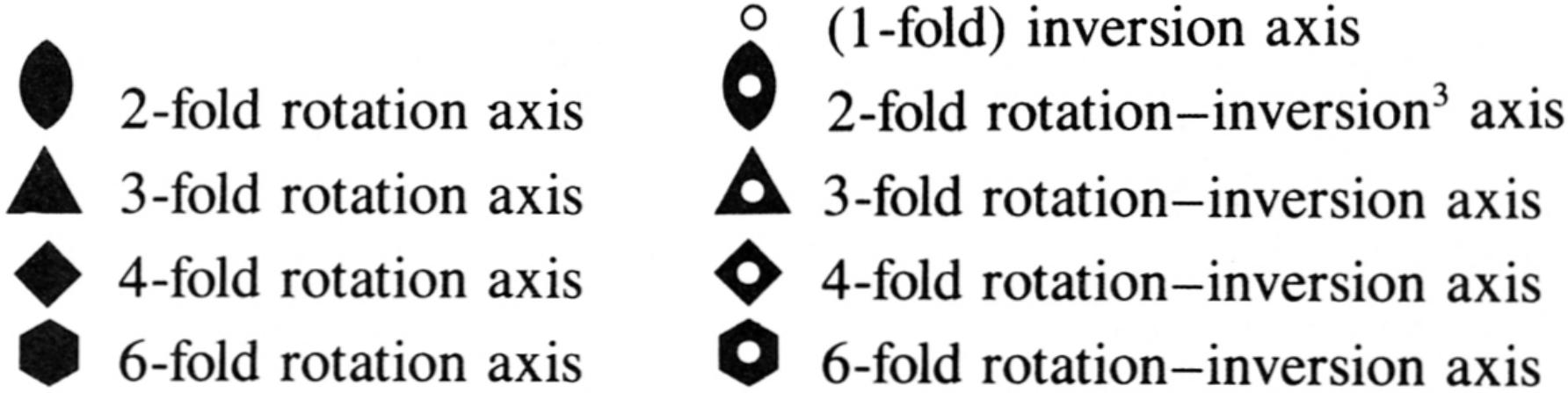

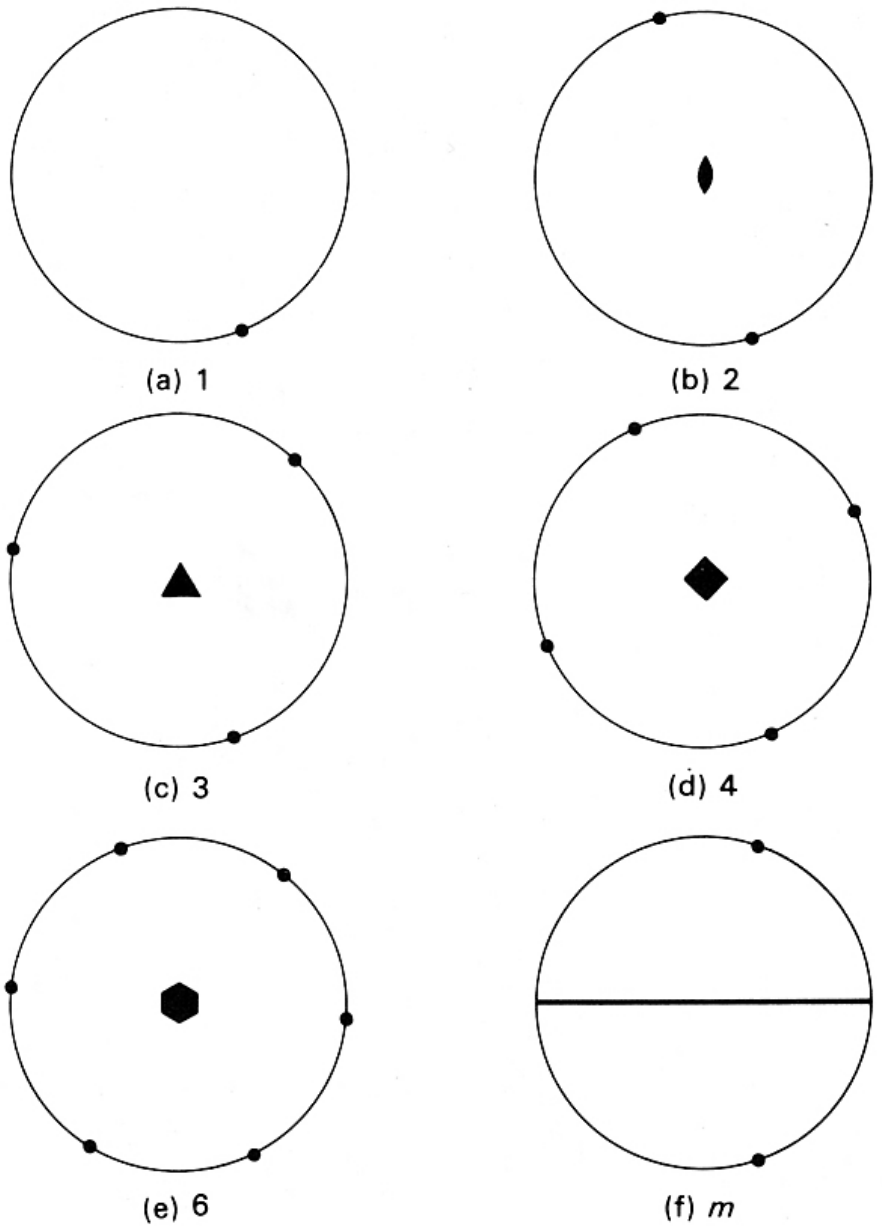

FIGURE 1.28. Stereograms of the point groups of the objects in Figure 1.27; the conventional graphic symbols for R and m are shown.

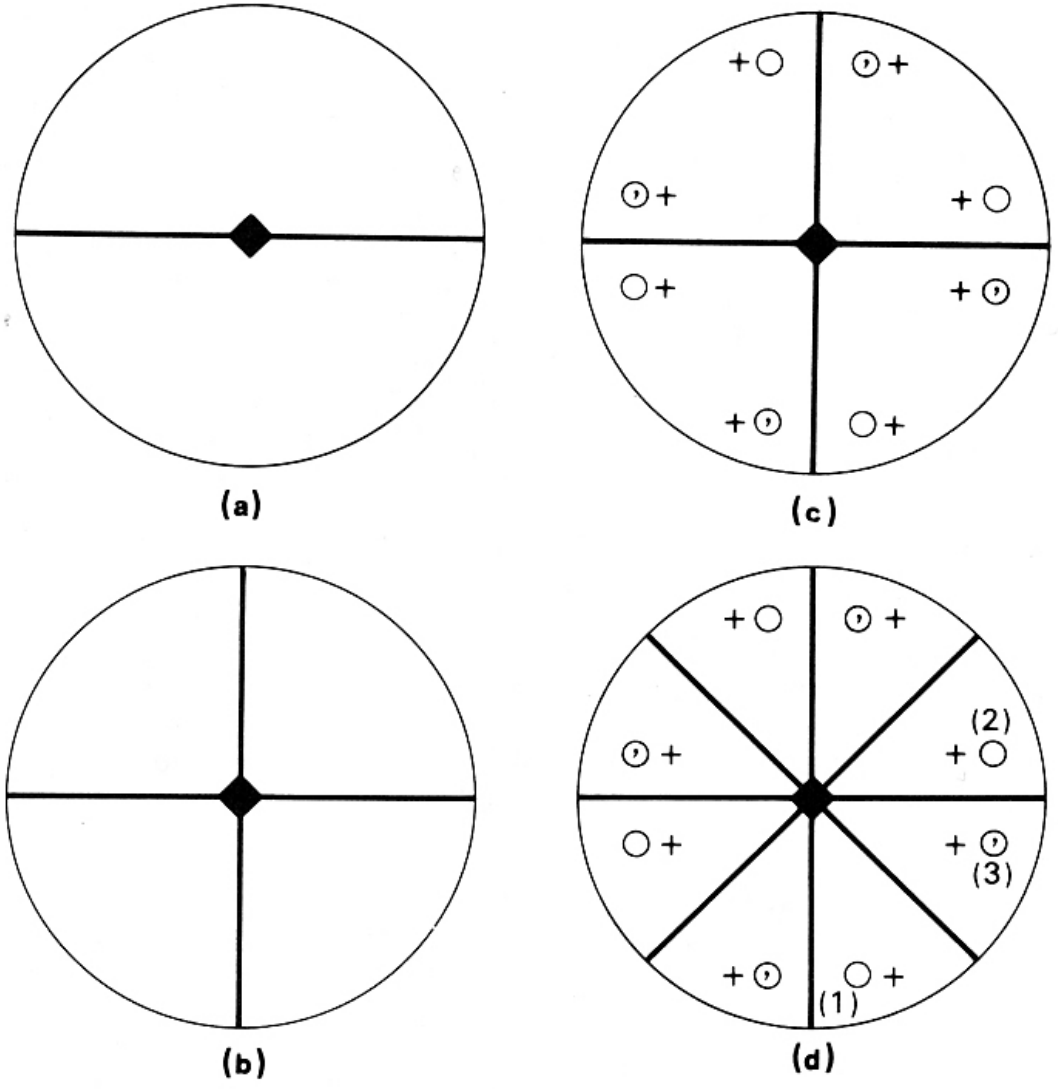

FIGURE 1.36. Intersecting symmetry elements: (a) one m plane is inconsistent with intersecting 4; (b) consistent; (c) points generated by $4m$; (d) complete stereogram ($4mm$).

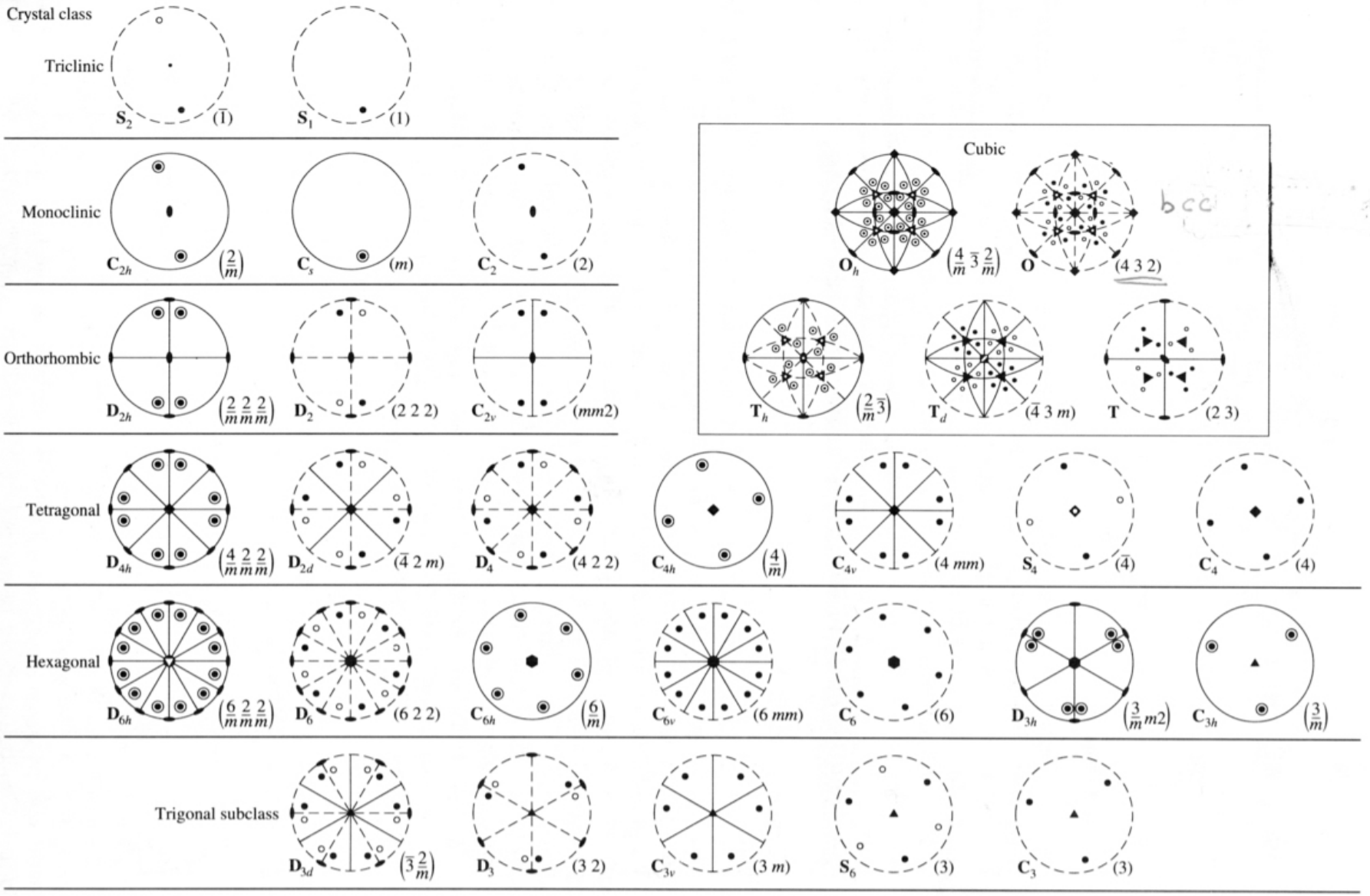

Figure 6.5 Crystallographic point groups.

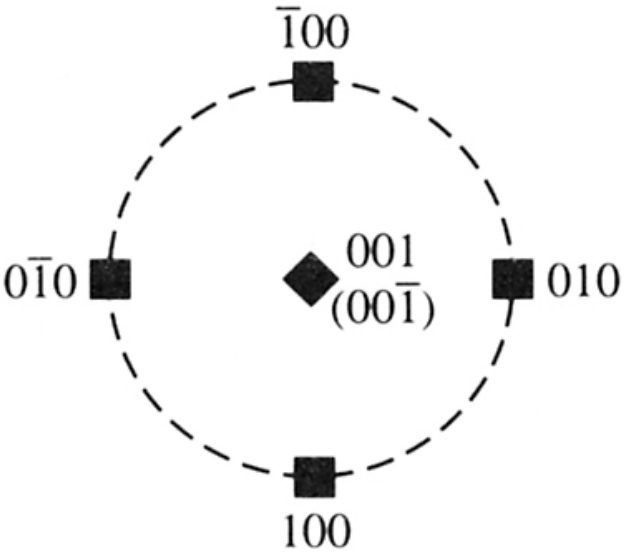

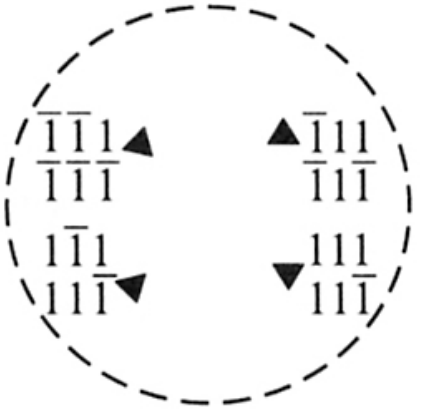

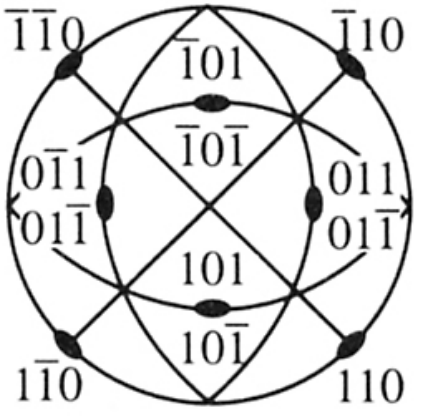

Special points in the Cubic System (**O** or **432**)

falling on rotational axes along with the Miller indices of the projection plane

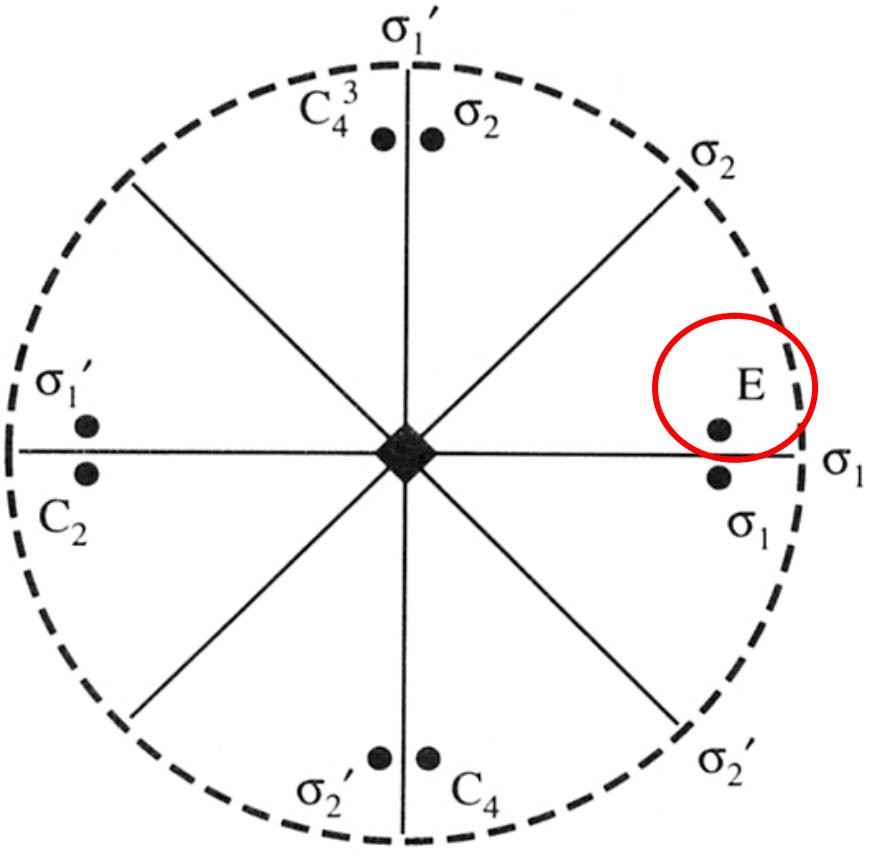

Stereogram of the C_{4v} group, with a general point E and the locations to which it is moved by the symmetry operations indicated.

Space Group- containing space symmetry operations

1) Screw Axes

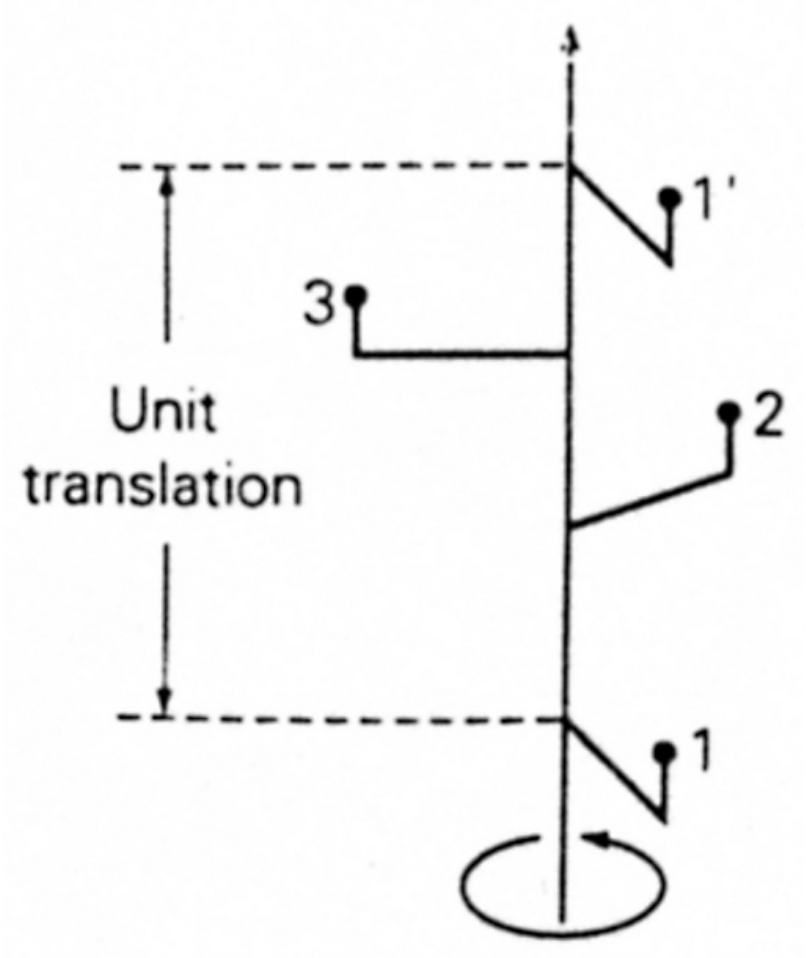

3_1 screw axis-
moving 1/3 distance
along one unit cell dimension,
then rotating for $2\pi/3$

2) Glide Planes

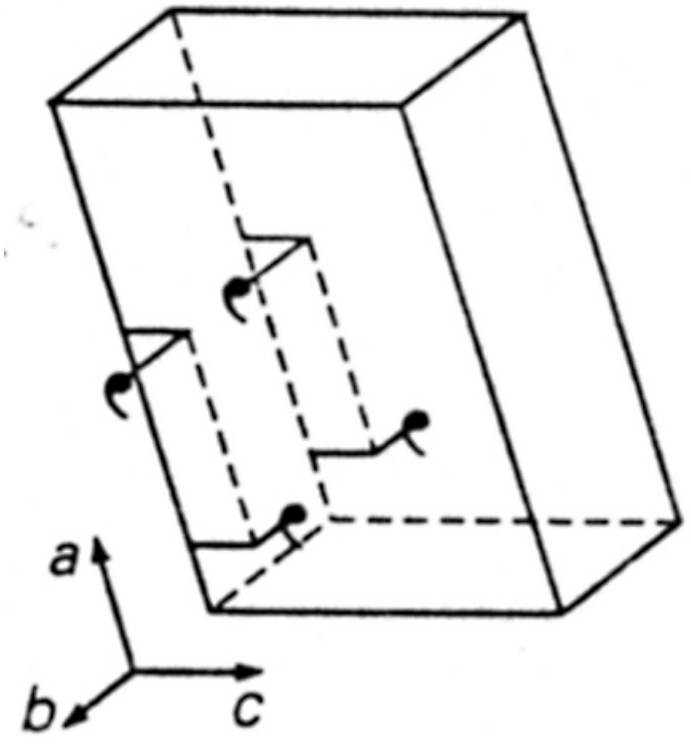

a glide-
moving 1/2 distance
along a-axis,
then reflecting versus ac-plane
(or ab-plane)

a, b, c glide-
moving **1/2** distance along a, b or c-axis, then reflecting

n glide-
moving **1/2** distance along **face-diagonal**, then reflecting

d glide-
moving **1/4** distance along **body-diagonal**, then reflecting

TABLE 2.5. Glide-Plane Notation

Symbol	Orientation	Graphic symbol: ∥ to projection	Graphic symbol: ⊥ to projection	Translational component
a	(010) or (001)	- - - - -	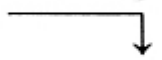	*a*/2
b	(100) or (001)	- - - - -	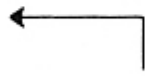	*b*/2
c	(100) or (010)	. . . . .	None	*c*/2
n	(100)	-.-.-.-		(*b* + *c*)/2
	(010)			(*a* + *c*)/2
	(001)			(*a* + *b*)/2

Lattice Centering—Pure Translation Symmetry

type			position
P	Primitive	1	(0,0,0)
I	Body center	2	(0, 0, 0); (1/2, 1/2, 1/2)
A	Base center	2	(0, 0, 0); (0, 1/2, 1/2)
B		2	(0, 0, 0); (1/2, 0, 1/2)
C		2	(0, 0, 0); (1/2, 1/2, 0)
F	Face center	4	(0, 0, 0); (1/2, 1/2, 0); (1/2, 0, 1/2); (1/2, 1/2,
R	Rhombohedral	3	(0,0,0) ; (2/3, 1/3, 1/3); (1/3, 1/3, 2/3)

Take Orthorhombic for example

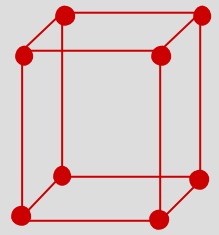

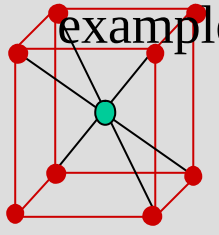

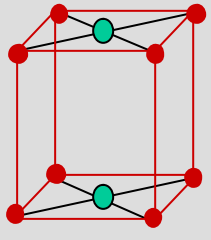

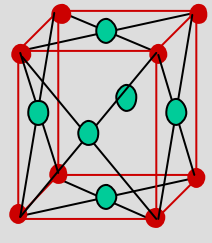

TABLE 17–4. Symmetry Elements and Reflection Conditions

Symmetry Element	Affected Reflection		Condition for Systematic Absence of Reflection
2-fold screw (2_1) 4-fold screw (4_2) } along 6-fold screw (6_3)	a	$h00$	$h = 2n + 1$ = odd
	b	$0k0$	$k = 2n + 1$
	c	$00l$	$l = 2n + 1$
3-fold screw (3_1, 3_2) 6-fold screw (6_2, 6_4) } along	c[a]	$00l$	$l = 3n + 1, 3n + 2,$ *i.e.*, not evenly divisible by 3
4-fold screw (4_1, 4_3) along	a	$h00$	$h = 4n + 1, 2,$ or 3
	b	$0k0$	$k = 4n + 1, 2,$ or 3
	c	$00l$	$l = 4n + 1, 2,$ or 3
6-fold screw (6_1, 6_5) along	c[a]	$00l$	$l = 6n + 1, 2, 3, 4,$ or 5
Glide plane perpendicular to	a		
translation $b/2$ (b glide)		$0kl$	$k = 2n + 1$
$c/2$ (c glide)			$l = 2n + 1$
$b/2 + c/2$ (n glide)			$k + l = 2n + 1$
$b/4 + c/4$ (d glide)			$k + l = 4n + 1, 2,$ or 3
Glide plane perpendicular to	b		
translation $a/2$ (a glide)		$h0l$	$h = 2n + 1$
$c/2$ (c glide)			$l = 2n + 1$
$a/2 + c/2$ (n glide)			$h + l = 2n + 1$
$a/4 + c/4$ (d glide)			$h + l = 4n + 1, 2,$ or 3
Glide plane perpendicular to	c		
translation $a/2$ (a glide)		$hk0$	$h = 2n + 1$
$b/2$ (b glide)			$k = 2n + 1$
$a/2 + b/2$ (n glide)			$h + k = 2n + 1$
$a/4 + b/4$ (d glide)			$h + k = 4n + 1, 2,$ or 3
A-centered lattice (A)		hkl	$k + l = 2n + 1$
B-centered lattice (B)			$h + l = 2n + 1$
C-centered lattice (C)			$h + k = 2n + 1$
Face-centered lattice (F)			$h + k = 2n + 1$ $h + l = 2n + 1$ $k + l = 2n + 1$ } *i.e.*, h, k, l not all even or all odd
Body-centered lattice (I)			$h + k + l = 2n + 1$

[a] Note that in the crystal classes in which 3- and 6-fold screws occur as cell axes, these are conventionally assigned to be c, so only the $00l$ reflections need be considered.

Space Group $P\,2_1$

primitive

Screw axis 2_1

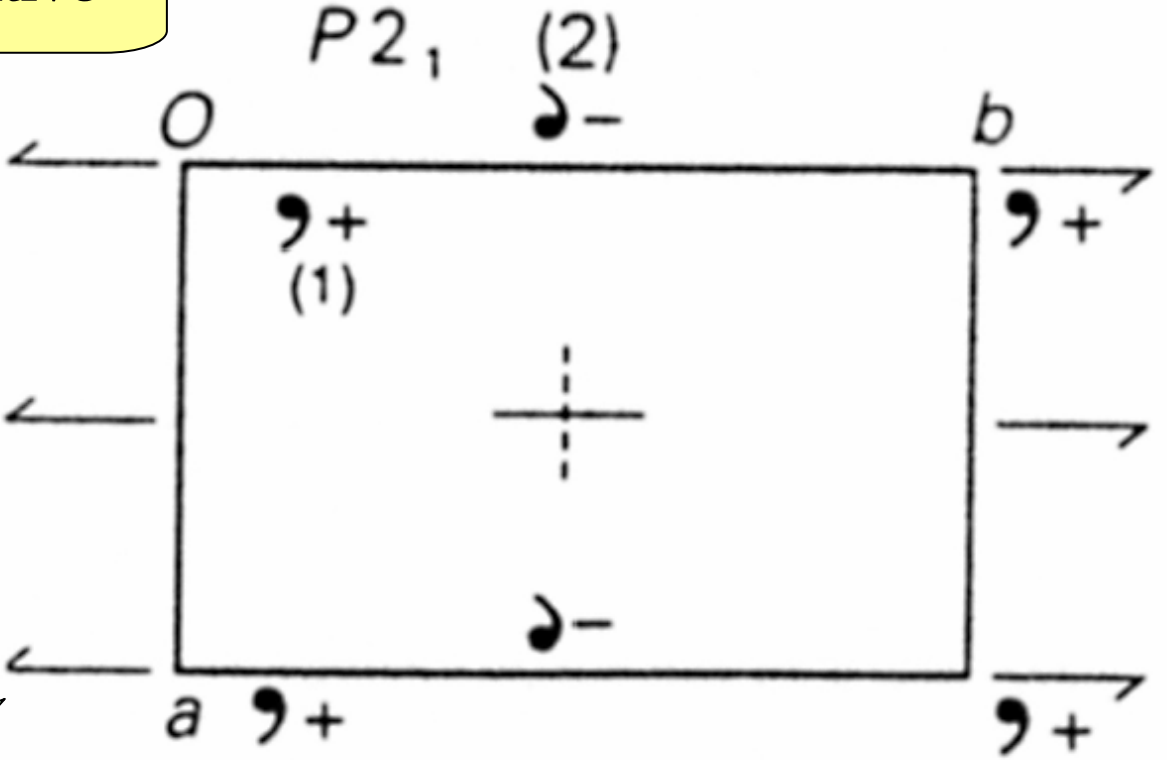

Screw axis

$P\,2_1$, equivalent positions

(1) x, y, z; (2) $\bar{x}, y + \frac{1}{2}, \bar{z}$

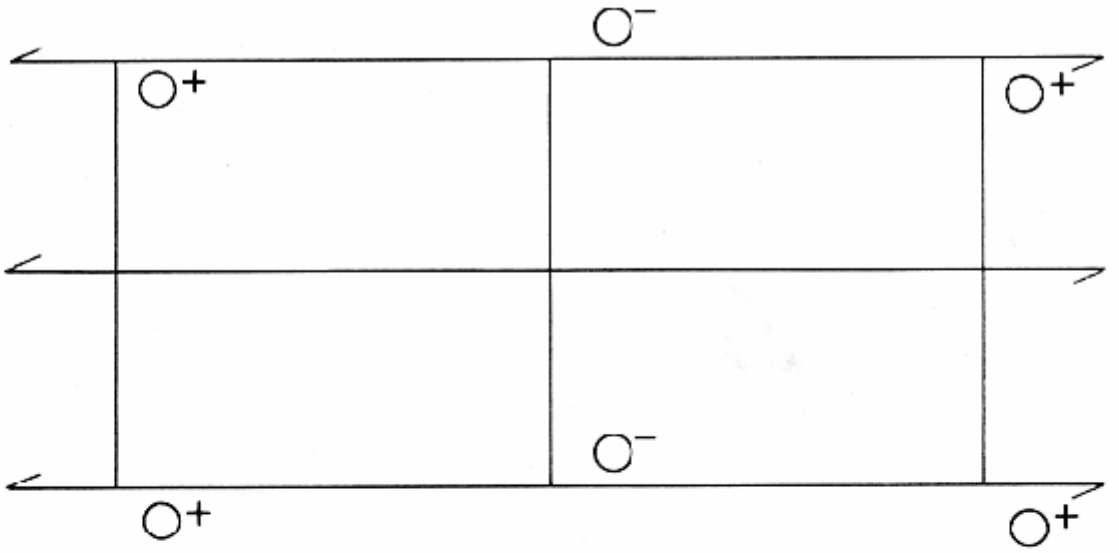

Origin on 2_1

					Limiting conditions
2	a	1	x, y, z;	$\bar{x}, \frac{1}{2}+y, \bar{z}$.	hkl: None
					$h0l$: None
					$0k0$: $k = 2n$

Symmetry of special projections

(001) $pg1(p1g1)$ (100) $p1g(p11g)$ (010) $p2(p211)$

FIGURE 2.30. Space group $P2_1$.

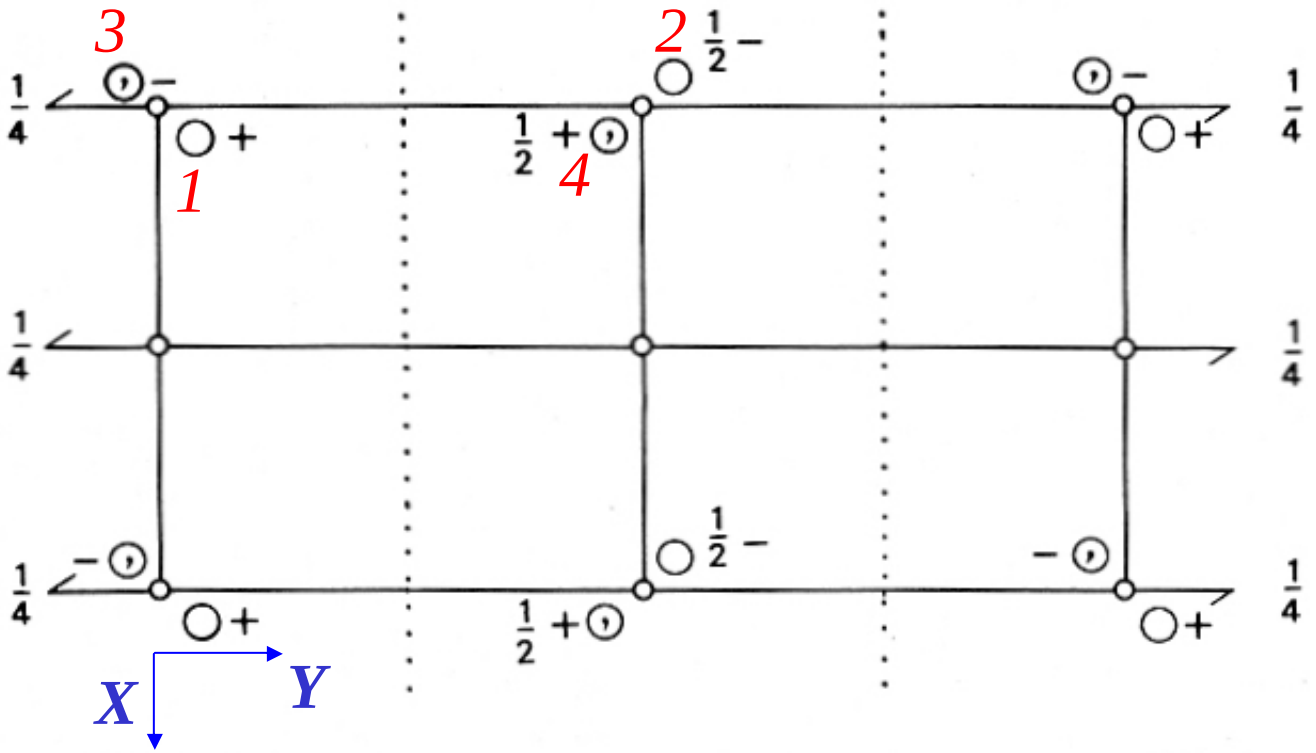

FIGURE 2.32. Space group $P2_1/c$ with the origin on $\bar{1}$ (standard setting).

$\bar{1}$ *at 0, 0, 0 (the origin)*

2_1 *parallel to the Y-axis, ¼ distance from ab-plane*

c (010), normal to the Y-axis

2_1 c

x, y,z (1) ® *-x, ½+y, ½ -z (2)* ® *-x, -y, -z (3)*

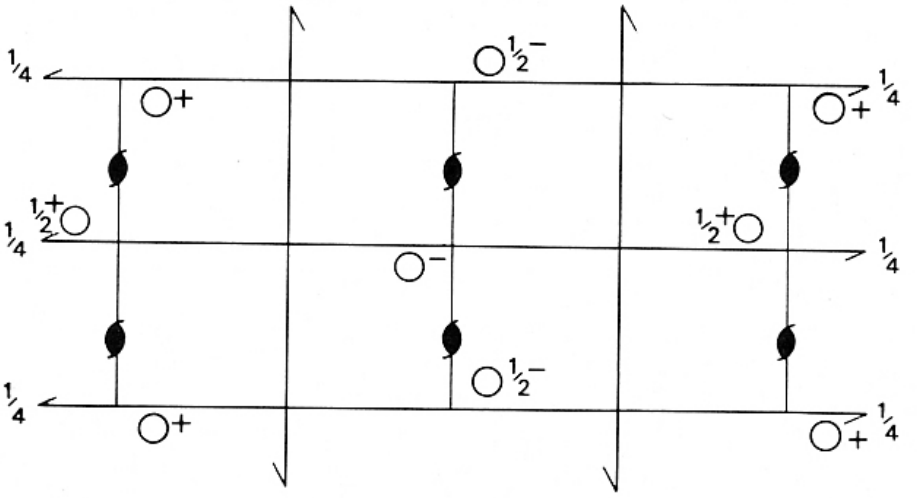

Origin halfway between three pairs of non-intersecting screw axes

Limiting conditions

4 *a* 1 x, y, z; $\frac{1}{2}-x, \bar{y}, \frac{1}{2}+z$; $\frac{1}{2}+x, \frac{1}{2}-y, \bar{z}$; $\bar{x}, \frac{1}{2}+y, \frac{1}{2}-z$.

hkl:
0kl:
h0l: } None
hk0:

*h*00: $h = 2n$

0*k*0: $k = 2n$

00*l*: $l = 2n$

Symmetry of special projections

(001) *p*2*gg* (100) *p*2*gg* (010) *p*2*gg*

FIGURE 2.35. Space group $P2_12_12_1$: in space-group diagrams, ◖ represents a 2_1 axis normal to the plane of projection.